Soil Dynamics and Earthquake Engineering 195 (2025) 109387

Contents lists available at ScienceDirect

Soil Dynamics and Earthquake Engineering

journal homepage: www.elsevier.com/locate/soildyn

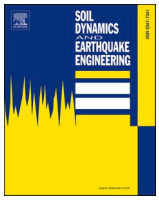

Stiffness-proportional foundation damping to linearise soil-monopile interaction models for wind turbines

Alessandro Tombari [a,*], Rohollah Rostami [a,d], Edward Mackay [b], M.H. El Naggar [c]

[a] University of Exeter, Harrison Building, Stocker Road, Exeter, EX4 4QF, United Kingdom
[b] University of Exeter, Penryn Campus, Penryn, TR10 9FE, United Kingdom
[c] Geotechnical Research Centre, University of Western Ontario, London, ON, N6A 5B9, Canada
[d] University of Strathclyde, James Weir Building, 75 Montrose Street, Glasgow, G1 1XJ, United Kingdom

ARTICLE INFO

Keywords:
Monopile
Offshore wind turbines
Soil-pile interaction
Linearized model
Stiffness-proportional damping

ABSTRACT

The structural design of offshore wind turbines must account for numerous design load cases to capture various scenarios, including power production, parked conditions, and emergency or fault conditions under different environmental conditions. Given the stochastic nature of these external actions, deterministic analyses using characteristic values and safety factors, or Monte Carlo Simulations, are necessary. This process involves a large number of simulations, ranging from ten to a hundred thousand, to achieve a reliable and optimal structural design.

To reduce computational complexity, practitioners can employ low-fidelity models where the soil-foundation system is either neglected or simplified using linear elastic models. However, medium to large cyclic soil-pile lateral displacements can induce soil hysteretic behaviour, potentially mitigating structural and foundation vibrations.

A practical solution at the preliminary design stage entails using stiffness-proportional viscous damping to capture the damping generated by the soil-pile hysteresis. This paper investigates the efficacy of this simplified approach for the IEA 15 MW reference wind turbine on a large-diameter monopile foundation subjected to several operational and extreme wind speeds. The soil-pile interaction system is modelled through lateral and rotational springs in which a constant stiffness-proportional damping model is applied.

The results indicate that the foundation damping generated by the nonlinear soil-pile interaction is significant and cannot be neglected. When fast analyses are required, the stiffness-proportional viscous damping model can be reasonably used to approximate the structural response of the wind turbine. This approach enhanced the accuracy of the computed responses, including the maximum bending moment at the mudline for ultimate limit design and damage equivalent loads for fatigue analysis, in comparison to methods that disregard foundation damping.

1. Introduction

Design standards such as IEC 61400 [1], p. 61] and ISO 19902 [2], p. 1 define requirements to ensure the structural integrity of wind turbines by considering a minimum number of design situations covering the most significant conditions that the wind turbine may experience during its planned lifetime. The design load cases (DLCs) are determined from design situations characterised by different sets of environmental conditions such as operating, extreme and abnormal conditions, according to the limit states (e.g., ultimate, serviceability, fatigue or accidental states) considered for the analysis.

Owing to the complex coupled dynamic interaction between the structural components of the wind turbines and the aerodynamical, hydrodynamical and actuation loads, more than 10,000 simulations are normally required in the analysis of different DLCs [3]. Although not every design load case is a governing factor for the design [4], keeping computational effort and time manageable for the conventional practice is paramount [5]. Low to high-fidelity models are used sequentially during the design process as more configuration and sizing choices are finalized. Low-fidelity modelling is applied to screen the optimal configurations at the conceptual stage, whilst high-fidelity modelling is required to finalise the design choice for selected load cases.

* Corresponding author.
E-mail address: A.Tombari@Exeter.ac.uk (A. Tombari).

https://doi.org/10.1016/j.soildyn.2025.109387
Received 30 September 2024; Received in revised form 3 February 2025; Accepted 15 March 2025
Available online 29 March 2025

Low-fidelity models such as the ones conventionally used in the past for design [6], or when an optimisation analysis is performed [7], usually did not account for soil structure interaction (SSI), so to strongly reduce the computational complexity. Nevertheless, capturing the SSI effects is an essential modelling task to ensure the reliable design of wind turbines; several studies (e.g., Refs. [8–10]) have shown the fundamental role of SSI, particularly in structures founded on monopiles, the most common type of offshore wind support structure in use, which are strongly sensitive to the soil-pile flexibility (e.g., Refs. [8–13]).

Therefore, different modelling approaches or reduction strategies were attempted to integrate the coupling effects between the wind field, wind turbine, foundation and subsoil, to solve the entire system of equations in the time domain. Damgaard et al. [5] used a coupled lumped parameter model, including frequency-independent spring and damping constants as well as point masses to capture the dynamic response of the soil-pile system; this simplified the computational complexity by condensing the entire pile-soil system ith few degrees of freedom as well as by using a linear viscoelastic soil model. Simplified approaches have also been developed by Jung et al. [14], who implemented a simplified coupled spring approach to investigate the dynamic response of the NREL 5 MW reference wind turbine [15] demonstrating that the impact of the SSI on the natural frequencies and the base moments could adversely affect its performance. Similarly, Damgaard et al. [16] and Løken and Kaynia [17] showed that the foundation flexibility could negatively impact the structural dynamic response as well as the fatigue life of the NREL 5 MW Reference wind turbine. The linear nature of the LPMs does not capture the actual behaviour of the soil-pile interaction; Simpson et al. [18] proposed a reduced order model for considering the nonlinear soil-pile interaction where the superstructure, i.e., tower and rotor-nacelle assembly (RNA), is replaced by equivalent forces and bending moments.

Alternatively, high-fidelity offshore foundation models have been proposed in the last decades based on the p-y approach (e.g., Refs. [13,19–25]) or full 3D finite element modelling (e.g., Refs. [13,26–29]). However, because of the computational complexity of these 3D finite element models, their use might not be viable at a preliminary design stage or for optimisation problems, where multiple simulations are performed.

Therefore, high-order models are used to calibrate simplified models such as the 1D effective model analysed by Versteijlen et al. [30], by using an effective small-strain stiffness. While this approach is effective for small-strain soil response, larger pile displacements generate soil-pile nonlinearities that result in a secant stiffness lower than the initial stiffness, which lengthens the fundamental period of the structure and increases the energy dissipation through the formation of hysteresis loops. As noted by Malekjafarian et al. [31], the role of soil damping strongly affects the overall wind turbine response.

A potential approach has been proposed by Versteijlen et al. [32], for their effective 1D model through the use of stiffness proportional damping characterized by a constant damping coefficient. This value was identified from shaker excitation in situ, representing the behaviour at small displacements. Similarly, Carswell et al. [33] captured the SSI effects through a coupled spring model that incorporates a viscous rotational dashpot to account for the hysteretic behaviour in a linearized model. The damping coefficient was computed based on the hysteretic energy loss at each cycle by adopting an iteration procedure between the linear structural model of the NREL 5 MW reference turbine and the nonlinear soil-pile model. The study showed the impact of the damping on the maximum bending moment of the tower at the mudline and the fatigue life of the structure.

Following this simplified approach, often used by practitioners, this study aims to investigate the efficacy of using stiffness-proportional viscous damping to approximately mimic the hysteretic damping effects of the soil-pile foundation system subjected to medium-large pile displacements. The stiffness-proportional viscous damping is applied uniformly to elastic soil-pile springs to capture the energy dissipated by the structure due to soil hysteresis. This investigation is based on time-history simulations of the International Energy Agency (IEA) 15 MW reference turbine [34] founded on a monopile. Compared to the linear equivalent approach, typically adopted to linearise the nonlinear problem through an iterative procedure (e.g., Refs. [35,36]), this study maintains constant soil elasticity to keep the computational complexity of the model low, and hence practical for preliminary design and optimisation analyses. Therefore, in combination with stiffness-proportional viscous dashpots for foundation damping, such simplified models enable thousands of faster analyses, facilitating reliability-based design approaches (e.g., Refs. [37,38]), or the seismic analysis of wind turbines (e.g., Ref. [39]).

2. High- and low-fidelity finite element models

2.1. Methodology

This study aims to evaluate the effectiveness of stiffness-proportional viscous damping in linearized low-fidelity soil-structure interaction models for approximating wind turbine responses. The accuracy of key responses, such as bending moments at the mudline and damage equivalent loads, is assessed by comparing results from these models to those obtained from high-fidelity nonlinear models. As a case study, the IEA 15 MW reference wind turbine [34] is considered. This reference turbine represents the latest design of next-generation wind turbines provided by the National Renewable Energy Laboratory (NREL) and the Technical University of Denmark (DTU). Therefore, assessing soil-foundation damping in relation to turbine dynamic performance is paramount for reliable design. The wind turbine model is created in Seismostruct [40], which incorporates structural flexibility, aerodynamic loads, and nonlinear SSI dynamics. Hydrodynamic loading is excluded from this analysis to isolate and evaluate the specific effects of wind loading on the foundation damping. Nonlinear simulations are conducted using the model of Fig. 1a to generate baseline responses at a few selected wind speeds. The nonlinear soil-pile responses are calibrated using a 3D high-fidelity model following a modified version of the PISA approach [41]. Sensitivity or optimisation analyses are performed to calibrate stiffness-proportional viscous damping coefficients, which are then used to linearise the wind turbine model (Fig. 1b).

2.2. Wind turbine model

The case study is based on the IEA 15 MW Offshore Reference Wind Turbine designed by the National Renewable Energy Laboratory (NREL) and the Technical University of Denmark (DTU), via the International Energy Agency Wind Task 37 [34]. The reference wind turbine is a 3-bladed upwind variable speed Class1B direct-drive machine with 117 m long blades and 240 m rotor diameter. The hub is located at 150 m above the mean sea level. The tower height is about 130 m with a base diameter of 10 m and a 6.5 m diameter at the top. The length of the monopile is 75 m with a constant outer diameter of 10 m. The monopile is embedded to a depth of L = 45 m in the sandy soil deposit. The transition piece is 15 m high and rigidly connected to the tower and monopile. Table 1 presents a summary of the main characteristics of the 15 MW reference wind turbine.

The two-dimensional model of the wind turbine in Fig. 1 is composed of beam elements for the tower, transition piece and pile, as well as link elements for modelling the soil-pile interaction. The rotor-nacelle assembly (RNA) is accounted for through eccentric masses linked rigidly to the tower. The influence of the induced rotational inertia of the RNA on the structural response to the gravity and wind loads is not negligible because of the geometric nonlinearities involved in the analysis.

An eigenvalue analysis was conducted to verify the computed first natural frequency in fore-aft motion of 0.164 Hz for the compliant base model against the value of 0.170 Hz from the designed reference model [34]. A Rayleigh damping of 2 %, was assigned to the first and second

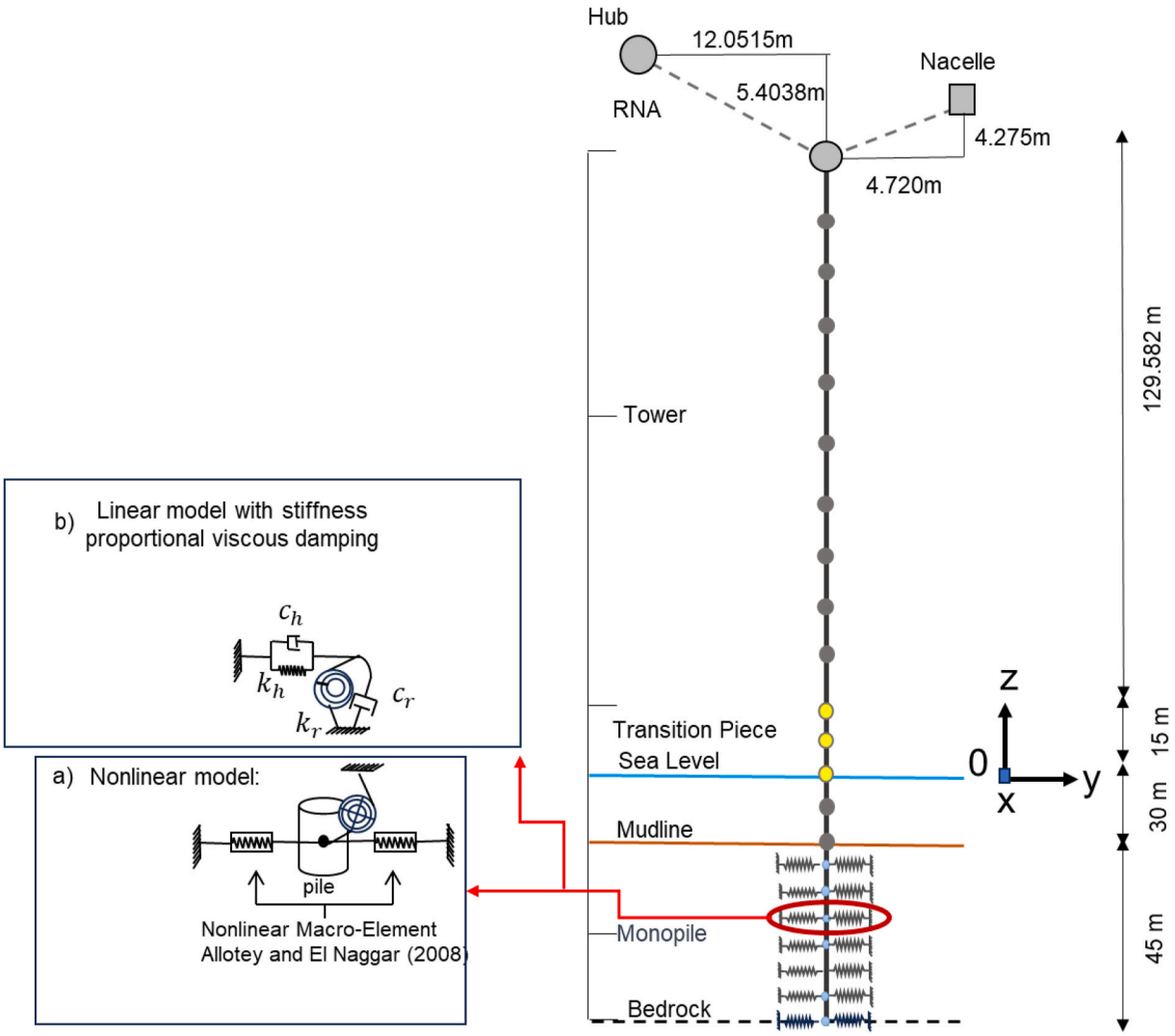

Fig. 1. Schematic of the IEA 15 MW Wind Turbine investigated in this paper; where the soil-pile reaction is described through a) nonlinear Allotey and El Naggar (2008) macro-element model, and b) linear model with stiffness proportional viscous damping.

Table 1
Main parameters of the IEA 15 MW Reference Wind Turbine.

Item	Value
Rated power (MW)	15
Rotor diameter (m)	240
Hub height (m)	150
RNA mass (t)	1017
Blade mass (kg)	65250
Nacelle mass (kg)	646895
Tower mass (t)	860
Tower base and top diameter (m)	10, 6.5
Tower base and top thickness (mm)	41.058, 23.998
Transition piece height (m)	15
Monopile depth (m)	75
Monopile embedment depth (m)	45
Monopile diameter (m)	10
Monopile base and top thickness (mm)	55.341, 45.517

fore-aft modes of the tower, to account for structural damping.

2.2.1. Soil deposit

The soil deposit considered in this analysis, illustrated in Fig. 2a, corresponds to the representative dense sand of the reference model [34]. An average shear modulus, G_0, of 140×10^3 kPa, and Poisson's ratio, $\nu_s = 0.4$, are provided to characterise the elastic spring model of the IEA 15 MW Offshore Reference Wind Turbine [34]. It is worth emphasizing that soil damping has not been considered in the reference study, as can occur in the preliminary design of offshore wind turbines. Thus, this study investigates the impact of neglecting the soil foundation damping and proposes a simplified approach to improve the model's accuracy.

The soil deposit determined in this study is discretised in 1m – thick layers characterised by a shear modulus, G_s, governed by the following relation:

$$G_s = G_0 \left(\acute{\sigma_m} \Big/ p_{ref}\right)^{0.6} \tag{1}$$

where $\acute{\sigma_m}$ is the mean effective stress and p_{ref} is the atmospheric pressure, as shown in Fig. 2b. The mean effective stress, $\acute{\sigma_m}$, is defined as

$$\acute{\sigma_m} = \frac{\acute{\sigma_v}\,(1 + 2K_0)}{3} \tag{2}$$

with effective vertical stresses, $\acute{\sigma_v}$, and earth pressure coefficient at rest, $K_0 = 1 - \sin(\varphi'_{cv})$.

The constant-volume angle of friction, φ'_{cv}, is fixed to 32° and the dilation angle, $\psi = 7.5°$, is assigned. Geotechnical parameters are re-

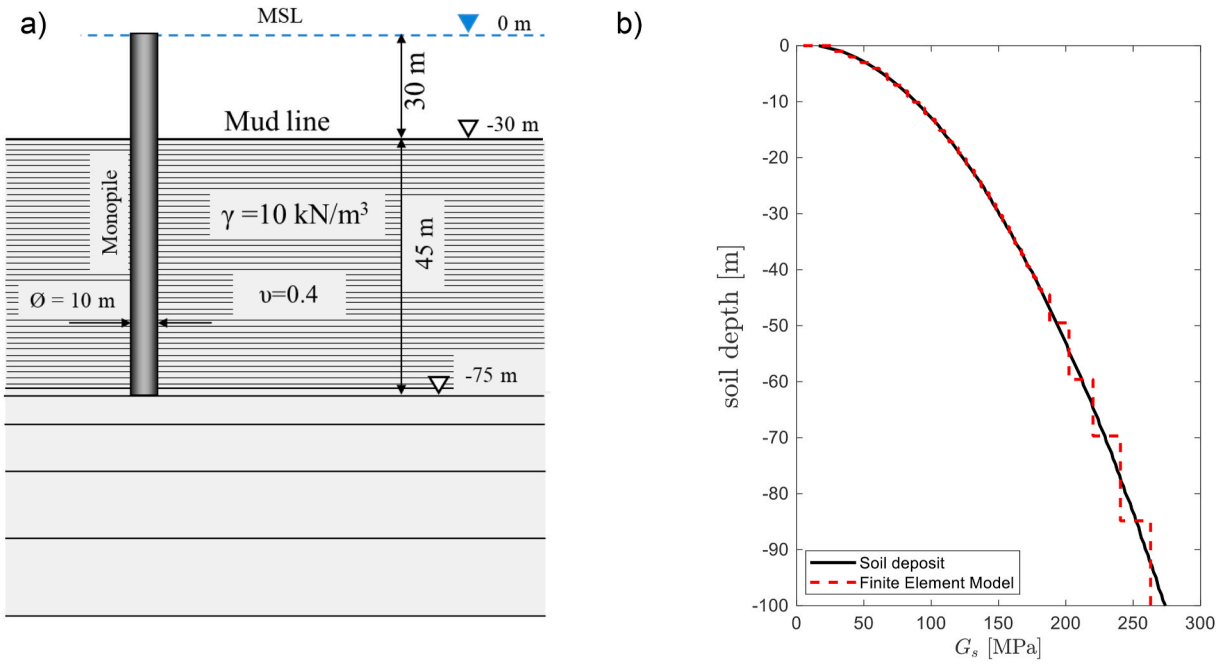

Fig. 2. Soil deposit: a) main parameters, and b) variation of the shear modulus with the depth.

ported in Table 2.

2.2.2. *Aerodynamical actions*

An uncoupled two-step procedure is used to consider the wind action. The first step involves the computation of the aerodynamic forces and moments by using the coupled nonlinear aero-hydro-servo-elastic OpenFAST code [42]. In the second step, the forces and moments are applied to the hub of the finite element model of Fig. 1. Following the IEC 61400 standards, an extreme turbulent model (ETM) is applied to simulate the full-field wind flow through the TurbSim code [43].

Several mean velocities at the hub height of 150m, ranging from 5 m/s to 50 m/s, are considered. In this investigation, two analyses, one deterministic and one stochastic, are conducted by generating the random time-history functions of the wind loading by the same seed and ten different seeds, respectively. Simulations are run for 720 s, with the first 120 s discarded to allow for the transient response, and the remaining 10-min steady-state dynamic response used for analysis. An example of a set of lateral fore-aft force, moment and vertical force applied at the hub level is shown in Fig. 3.

2.3. Nonlinear baseline SSI model

The baseline wind turbine model used to verify the proposed three-step procedure of Section 2.1 uses an extended version of the Allotey and El Naggar [44] generalized model to capture the soil-large diameter pile interaction through translational and rotational macro-elements. These link elements, shown in Fig. 1a, are placed on both sides of the pile to capture any eventual gapping and slack zone behaviour.

The calibration of the model parameters to define the backbone curve of each Allotey and El Naggar's macro-element follows a revised version of the PISA approach [41], which was proposed to improve the design of offshore large-diameter piles as the monopile foundation of the IEA 15 MW Wind Reference Turbine investigated in this study. The proposed model incorporates the traditional lateral p-y curves, along with the additional rotational resistance generated by the shear stresses along the pile surface. Accordingly, the generalized model of Allotey and El Naggar is also used to simulate the cyclic moment-rotation behaviour through nonlinear rotational springs.

Table 2
Main parameters of sandy soil deposit.

Parameter	Value
Effective unit weight, $\acute{\gamma}$ (kN/m^3)	10
Poisson's ratio, ν_s	0.4
Effective internal friction angle, φ'_{cv} (°)	32
Dilation angle, ψ (°)	7.5
Friction coefficient at pile-soil interface, μ	0.4
Earth pressure coefficient at rest, K_0	0.47

2.3.1. *Allotey and El Naggar's model for lateral force-displacement and moment-rotation responses*

The dynamic Beam on Nonlinear Winkler Foundation (BNWF) model developed by Allotey and El Naggar [44] is compression-dominant and, hence, requires two elements at each depth for the modelling of soil-pile interaction to capture gaps and slack zone formation. The hysteretic model is defined by rules to determine four types of soil-pile responses illustrated in Fig. 4: i) the monotonic response at the first cycle (continuous curve), ii) unloading (dashed curve), iii) the standard reloading (dash-dotted curve), and iv) the direct reloading (dotted curve). These four curves are governed by the model parameters reported in Table 3, which are calibrated to capture several soil-type responses such as O- and S-shape responses (for dry and saturated soil, respectively) and brittle behaviour (for stiff clays). The backbone curve defines the monotonic response at the first cycle, and its parameters (k_0, P_y, P_c, P_u, α, β) are calibrated to best fit any numerical or analytical soil-pile lateral force-displacement (P-Y), and in this study, for moment-rotation (M-R) relationships as well. For the latter, the parameters are expressed as rotational stiffness and moment capacity values. The general unloading curve occurs when the load is reversed and follows the original backbone curves scaled by a factor α_n obtained by best-fitting numerical or experimental cyclic tests ($\alpha_n = 1$ in this study). The standard reload curve is used to simulate oval-shaped hysteresis and follows the original backbone curve, with degradation not considered in this study. The direct reload curve is applied when soil-pile gapping or soil-pile weathering (slack zone) occurs. The cyclic curve parameters (p_1,p_2,e_{p1}) are usually heuristically fixed according to the soil type behaviour. For saturated sand, in which a S-shape hysteresis loop is expected on the upper part of the pile because of the formation of

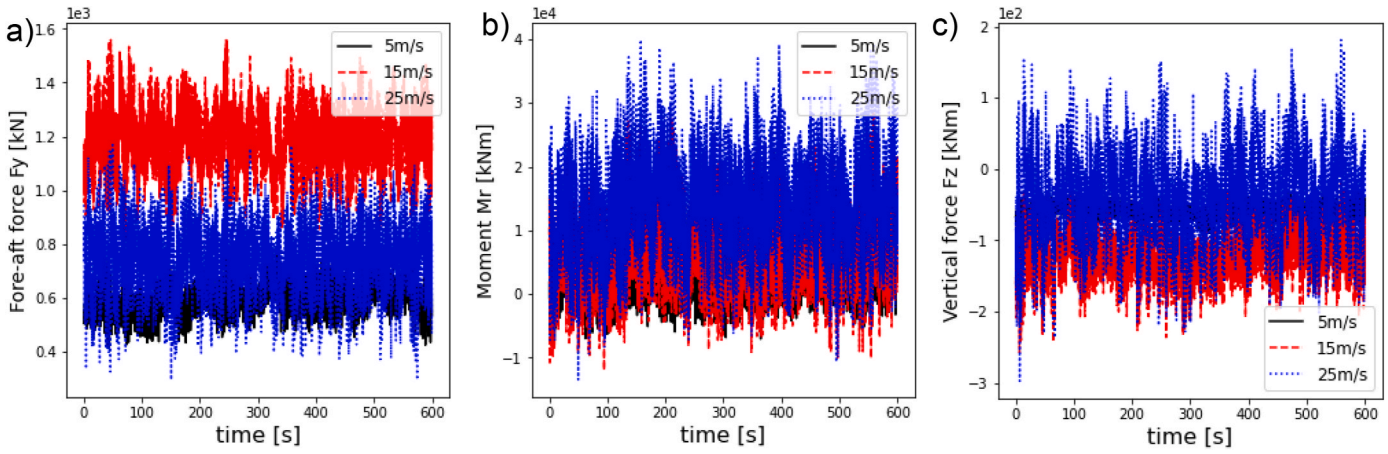

Fig. 3. Example of steady-state aerodynamic forces and moments for three different wind speeds.

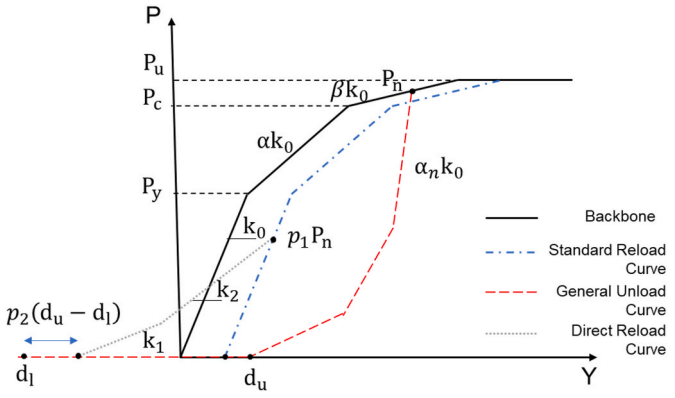

Fig. 4. Schematic of the Allotey and El Naggar (2008)'s model for cyclic loading.

Table 3
Parameters for fully defining the Allotey and El Naggar (2008a) model.

Backbone Curve	Cyclic curve parameter
Initial stiffness (k_0)	soil cave-in (p_2)
Yielding force (P_y)	DRC stiffness ratio ($e_{p1} = k_2/k_1$)
Turning soil strength (P_c)	gap force (p_1)
Ultimate soil strength (P_u)	
Stiffness ratio of the 2nd branch (α)	
Stiffness ratio of the 3rd branch (β)	

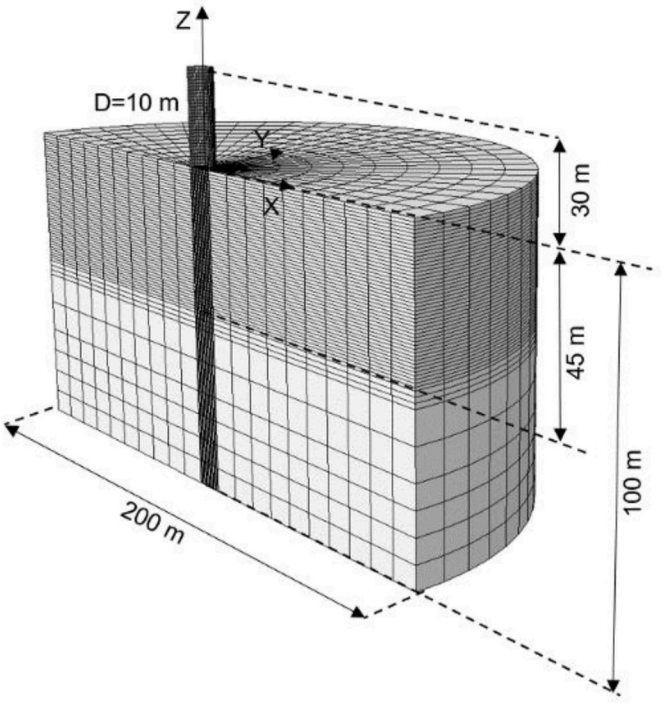

Fig. 5. Numerical soil-pile finite element model used to compute the soil-pile reaction forces and moments.

a slack zone, typical values are: $p_1 = 1$ (no gap), $0 \leq p_2 \leq 5$ and $0 \leq e_{p1} \leq 1$, for the upper one-third part of the pile and $p_2 = 5$, $e_{p1} = 1$, for the lower part of the pile. The cyclic behaviour of this model intrinsically generates a hysteretic, strain-dependent, damping without the need to define further coefficients governing the energy dissipation. An exhaustive description of the Allotey and El Naggar model can be found in Refs. [44,45].

2.3.2. *Numerical soil reaction curves*

Following the PISA approach [41], the soil reaction curves are obtained numerically from 3D finite element modelling and then, each curve is normalised and parameterised to be dimensionless. In this paper, the 3D symmetric finite element model (see Fig. 5) is built using the software Abaqus [46]. A sandy soil deposit of 100 m is considered in this study, in which the shear modulus increases with the depth as depicted in Fig. 2b.

The constitutive behaviour of the soil is simulated employing the Mohr-Coulomb failure criterion, with the soil geotechnical properties reported in Table 2. An 8-node linear reduced integration solid element is used for constructing the finite element model of the soil, whilst 4-node shell elements are used for the pile. The soil–pile interface is modelled using surface-to-surface contact behaviour. The tangential contact behaviour at the interface was modelled using the Coulomb friction law with a friction coefficient, of μ equal to 0.4. Symmetric boundary conditions are used to reduce the number of degrees of freedom of the system. Initially, a geostatic stress field to consider the gravity effect is applied. The pile is then loaded by incrementally increasing the horizontal displacement at the pile top in the X-direction for a maximum displacement of 1.5 *m*.

Fig. 6a shows the profile of the maximum pile deformation, revealing that the pile manifests a flexural behaviour, and cannot be considered "short" or rigid. Fig. 6b presents the lateral soil-pile reaction obtained at the maximum push-over load, depicted through a dashed red curve. It is worth noting that the curves represent the responses used to calibrate

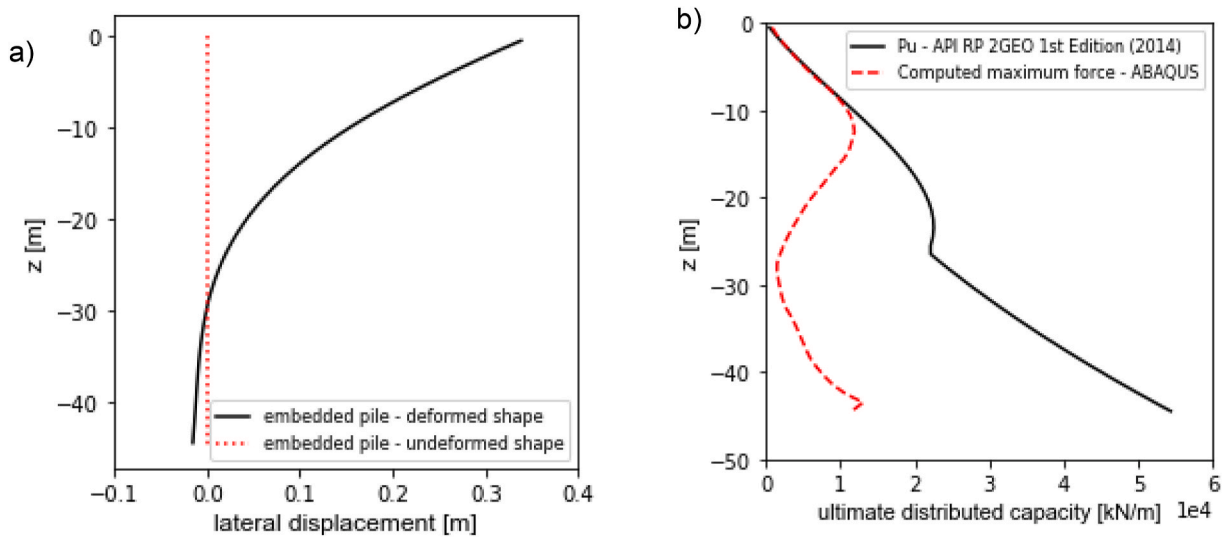

Fig. 6. Results of the incremental push-over, a) Lateral displacement and b) ultimate lateral soil-pile capacity.

the nonlinear spring model and hence, are obtained considering a discretisation of 1 m. The maximum value does not always indicate the soil yielding as indicated by the numerical soil-pile lateral force-displacement (P-Y) and moment-rotation (M-R) relationships in Fig. 7. It is interesting to note that for the specific case, the ultimate capacity computed through the API formulation for sand [47] at shallow depth can accurately be used for estimating the lateral soil capacity, Better prediction of the ultimate capacity can be obtained by using the wedge method proposed by Sun et al., [28] where the effect of the pile diameter is also accounted for through an analytical formulation.

2.3.3. Parametric backbone curves

The numerical soil reaction curves of Fig. 7 are used to calibrate the Allotey and El Naggar's macro-elements to provide a predictive capability at different loading conditions. The numerical curves are first normalised and then fitted to the three-branch backbone curve defined by the macro-element. In this section, two different approaches for normalising the curves are examined: the maximum numerical value for each curve is used as the normalising factor of the lateral and rotational response, referred to as Method A; whereas Method B defines a quantity proportional to the ultimate capacity, p_u, as the normalising factor. The latter can be obtained analytically through the API-recommended practice [47] guidelines, as follows,

$$p_u = min(p_{us}, p_{ud}) \bullet \Delta z \tag{3}$$

$$p_{us} = (C_1 \bullet H + C_2 \bullet D) \bullet \gamma \bullet H \tag{4}$$

$$p_{ud} = (C_3 \bullet D) \bullet \gamma \bullet H \tag{5}$$

where, p_{us} and p_{ud}, are the shallow and deep ultimate resistance respectively, γ is the effective soil unit weight, D is the pile diameter and C_1, C_2, and C_3 are coefficients as a function of the frictional angle φ. The coefficients C_1, C_2, and C_3 are determined by the following equations:

$$C_1 = \tan(\beta) \bullet \left[(\tan\beta)^2 \bullet \tan\left(\frac{\varphi}{2}\right) + K_H \left[\tan(\varphi) \bullet \sin\beta \bullet \left(\frac{1}{\cos\left(\frac{\varphi}{2}\right)} + 1 \right) \right] - \tan\left(\frac{\varphi}{2}\right) \right] \tag{6}$$

$$C_2 = (\tan\beta)^2 - \left[\tan\left(-\frac{\varphi}{2} + \frac{\pi}{2} \right) \right]^2 \tag{7}$$

$$C_3 = (\tan\beta)^4 \bullet \left[(\tan\beta)^2 + K_H(\tan\varphi) \right] - \left[\tan\left(-\frac{\varphi}{2} + \frac{\pi}{2} \right) \right]^2 \tag{8}$$

in which $\beta = \frac{\varphi}{2} + \frac{\pi}{2}$ and K_H is the coefficient of lateral earth pressure.

Therefore, the normalising factor is:

$$\rho_f = \begin{cases} \max[P(y)], \text{Method A} \\ p_u, \text{Method B} \end{cases} \tag{9}$$

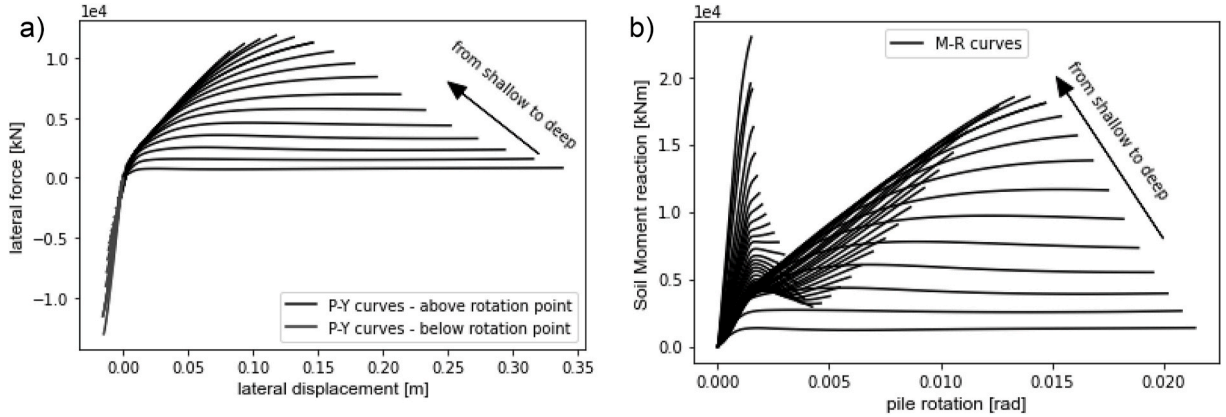

Fig. 7. Numerical soil-pile reactions: a) lateral force and b) moment relationship for several depths.

for the numerical lateral force – displacement curves, $P(y)$.

For the moment-rotation curve, $M(\phi)$, the normalising factor is defined as:

$$\rho_m = \begin{cases} \max[M(\phi)], \text{Method A} \\ \alpha_f p_u, \text{Method B} \end{cases} \quad (10)$$

where $\alpha_f = 1.55$ is a constant obtained empirically to match the ultimate moment capacity.

For both methods, the normalising factor for displacements and rotations is set as:

$$\rho_d = \frac{1}{\gamma z D} \quad (11)$$

The normalised lateral and moment responses are depicted through black-dashed curves in Fig. 8 for the upper 10m soil, where the capacity is mobilised under a top pile displacement of 15 % of the pile diameter.

Parametric soil reaction curves, based on the Allotey and El Naggar model parameters, are obtained from the normalised responses. The values of the parameters of the backbone curve, P_y, P_c and P_u, listed in Table 3, are obtained through a least-squares fit of the normalised curves. For Method A, several parametric curves are obtained as a function of the initial stiffness value, k_0, which is computed for each normalised curve, while block averaging is done for Method B. The resulting parametric curves are shown in Fig. 8 as a solid red line. The dimensional parametric curves, obtained by multiplying the non-dimensional values for the normalising factors, are shown in Fig. 9. The dimensional curves evidence an acceptable matching using both methods; in this study, despite Method A being more accurate, Method B, which is governed by analytical expressions, has been used to set up the parameters of the model of the investigated wind turbine of Fig. 1a, so to extrapolate the values for larger depths.

2.4. Linearized model with stiffness-proportional viscous damping

The baseline model adopted in the current study is a high-fidelity soil-pile model that involves a dynamic BNWF model comprising uncoupled lateral-rotational macro-elements as depicted in Fig. 1a. To reduce the running time, a low-fidelity model is established by replacing the nonlinear macro-elements with an uncoupled Kelvin-Voigt system defined by linear lateral and rotational springs and dashpots, as illustrated in Fig. 1b. The stiffness values, k_y and k_r, are equal to the initial stiffness values of the lateral and rotational springs of the nonlinear macro-element, respectively. The lateral and rotational dashpots are described via a linear viscous relation, in which the damping coefficient is proportional to the stiffness values. The generated damping force, F_d, and damping moment, M_d, from each spring-dashpot unit, are described by the following relations:

$$\begin{cases} F_d = \beta k_y \bullet v_y \\ M_d = \beta k_r \bullet \theta_x \end{cases} \quad (12)$$

in which v_y and θ_x are the translational and rotational velocities; β is the stiffness proportional coefficient, also referred to in this paper as the foundation damping coefficient.

The stiffness proportional coefficient, β, is uniquely determined for all the lateral and rotational springs of the model. This represents an oversimplification of the problem because springs at different depths are subjected to different deformations and dissipate energy in different quantities; therefore, differently from the equivalent linear formulation, the damping forces and moments of Eq. (12) are governed by a constant viscous coefficient, β, that has been tuned to match the dynamic characteristics of the linear model with those of the nonlinear model.

The advantage of the proposed methods lies in having a unique coefficient to be determined and not requiring the condensation of the soil-pile system in a lumped parameter model which is formally exact only

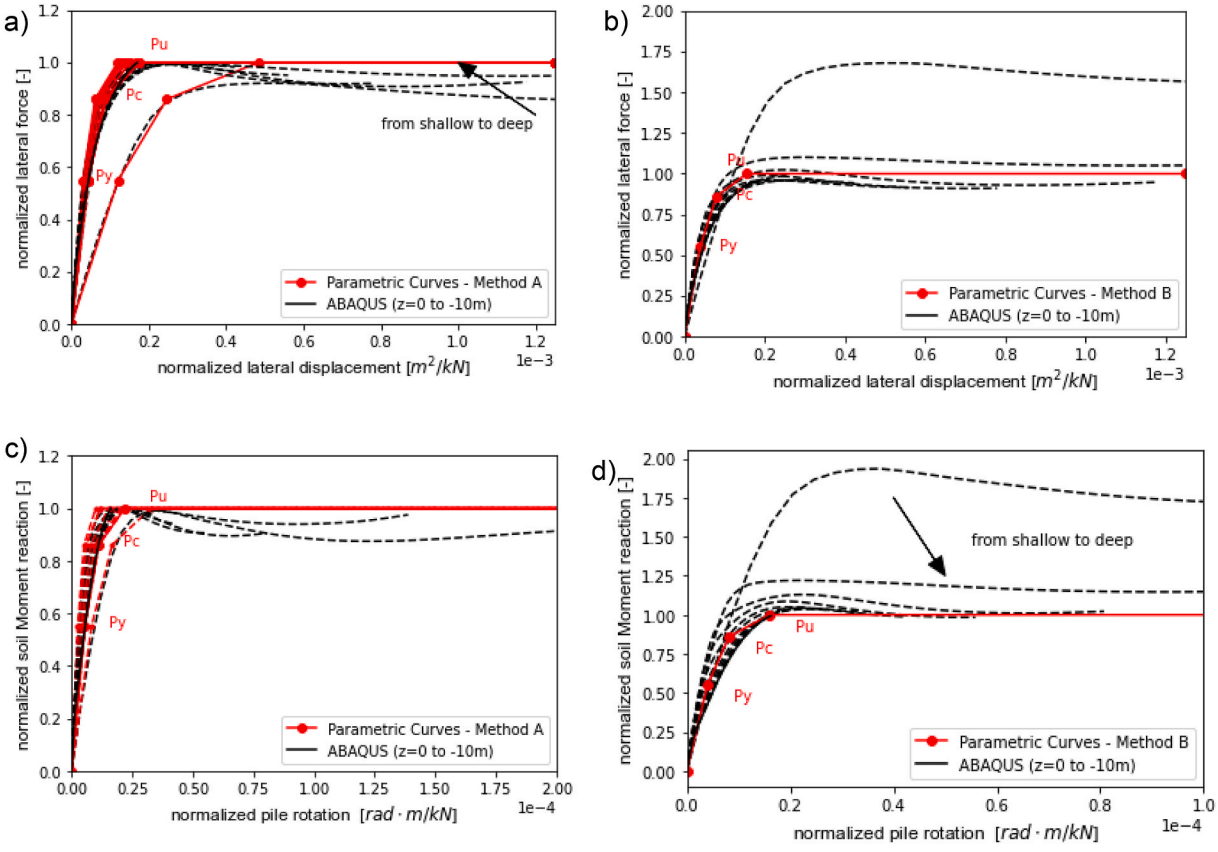

Fig. 8. Normalised curves for force-displacement and moment-rotation curves using a-c) Method A and b-d) Method B.

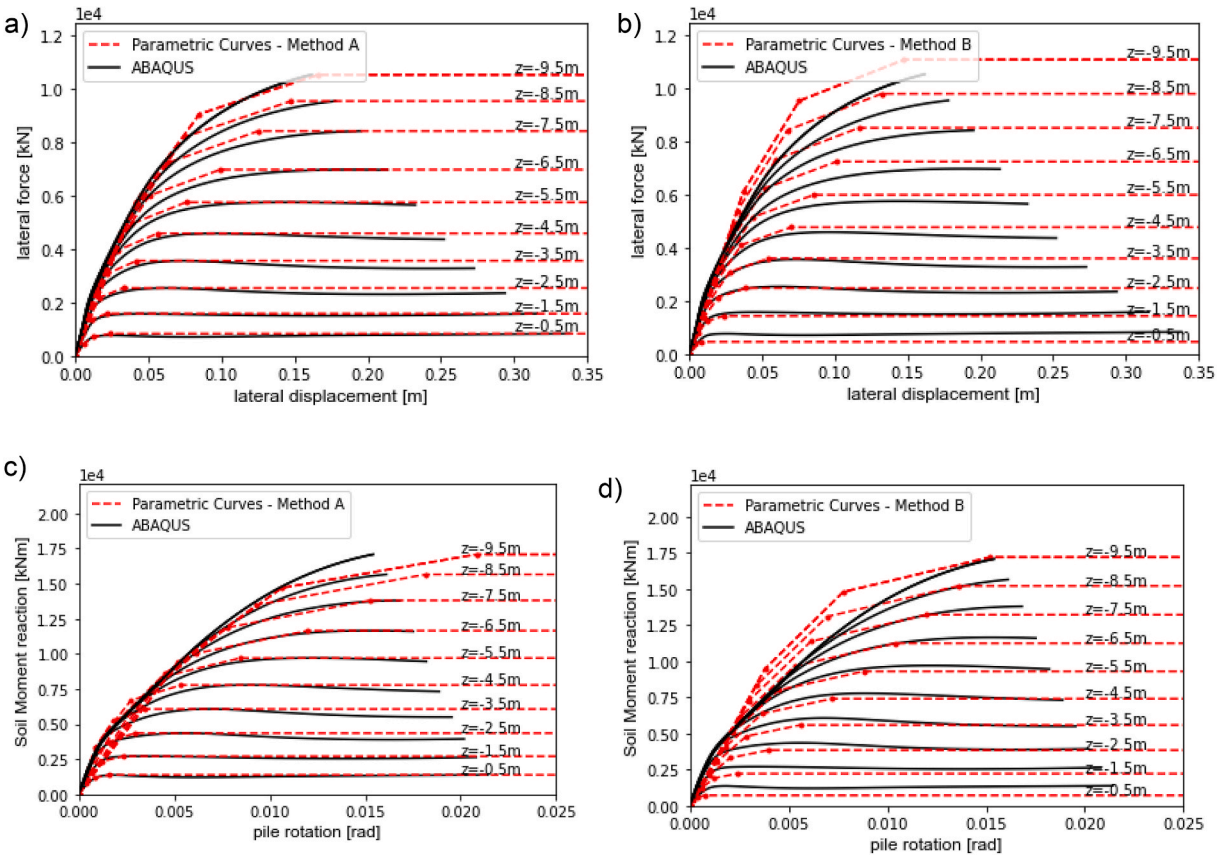

Fig. 9. Dimensional parametric curves using a-c) Method A and b-d) Method B.

when frequency-dependent impedances are used [48].

The calibration of the stiffness proportional coefficient, β, can be calibrated using either a fast sensitivity analysis or a more precise but time-consuming optimisation procedure to match the wind turbine's performance. However, the computational efficiency of the linear model is significantly higher than that of its nonlinear counterpart.

The coefficient, β, is calibrated for a suitable range of velocities to approximate the performance of the wind turbine; in this investigation, two metrics are used for the optimisation problem, the maximum bending moment at the mudline and the damage equivalent load (DEL) corresponding to the mudline bending moment, for fatigue analyses [49].

The DEL is defined herein as follows:

$$DEL = \left(\frac{1}{N_e} \sum_{i=1}^{N} S_i^m \right)^{\frac{1}{m}}, \tag{13}$$

in which S_i^m the equivalent fatigue load range taken as the bending moment at the mudline at each equivalent cycle $i = 1, \ldots, N$, N_e is the total number of equivalent cycles during the lifetime, here taken as 2×10^8, and m is the negative slope of the $CSR - N_U$ curve of the material, here taken equal to 4 [49]. In this study, the ratio between the DEL of the nonlinear and linear models is considered, hence, the lifetime cycle parameter, N_e, does not affect the results.

3. Wind turbine responses using the stiffness-proportional viscous damping

3.1. Baseline response

The response to the wind load of the baseline model defined in Section 2.2 considering the nonlinear soil-pile is presented in terms of maximum bending moment at the mudline and damage equivalent load [49], which are used as target values for the optimisation of the stiffness proportional damping coefficient. These outputs are important parameters in the design of the wind tower and monopile.

The envelopes of the bending moment of the wind tower and monopile are displayed in Fig. 10 for several wind speeds; for low wind speeds, Fig. 10a shows an asymmetry of the distribution of the moments because of the predominant effect of the static component of the wind thrust in the tower deflection. For higher speeds, Fig. 10b reveals that the dynamic effects become more relevant as they induce fluctuations in the tower and generate more symmetric distributions. This is also evident from the results presented in Fig. 11 which shows the mean and standard deviation in the bending moment at the mudline, over the time history. The mean component (Fig. 11a) corresponds to the response to an equivalent static thrust and the standard deviation (Fig. 11b) corresponds to the fluctuations due to turbulence.

It is worth noting that the maximum bending moment is reached at 10 m/s close to the rated wind speed when the turbine is generating its maximum capacity, and then decreases with increasing wind speed, as the blades are feathered to reduce thrust while maintaining constant power output. The variability in the loading increases with the wind speed since under the turbulence model used in the simulations the fluctuations in the wind speed are increased in proportion to the mean wind speed. Comparison with the responses obtained from the linear model with zero soil-foundation damping (i.e. $\beta = 0$) is also shown in Fig. 11. The results in terms of mean bending moment are similar evidencing the low impact of the soil nonlinearities on the soil-pile rigidity mainly affected by the static component of the thrust. A slight difference can be observed for the case of the mean wind speed of 10 m/s, where the impact of the wind loading on the bending moment is maximum. On the other hand, the standard deviation values, mainly caused by the randomness of the turbulent component of the wind load,

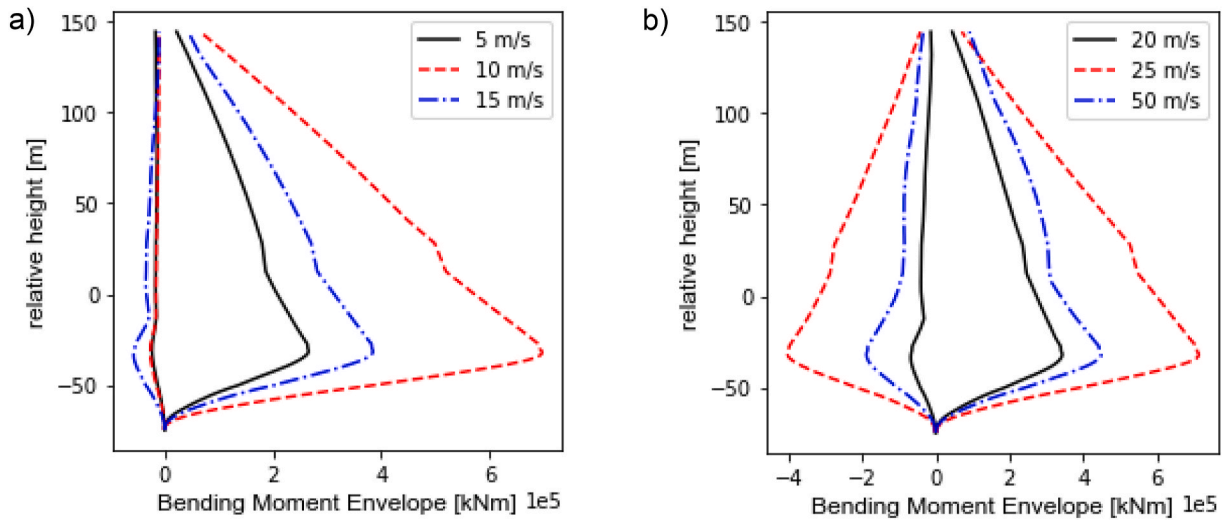

Fig. 10. Envelopes of the bending moment of the entire wind turbine for several wind speeds.

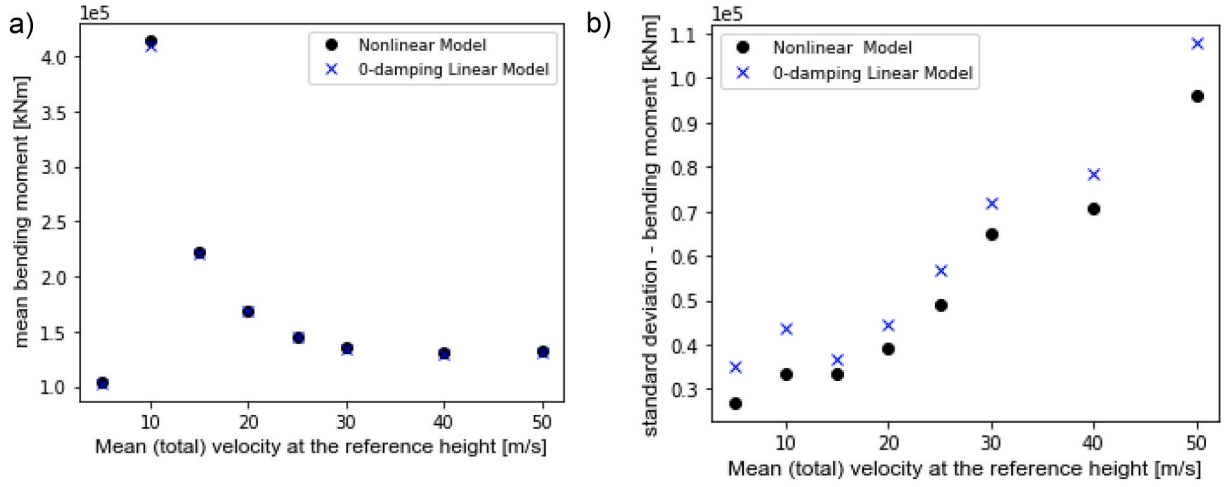

Fig. 11. Variation of the a) mean and b) standard deviation of the bending moment time history at the mudline with mean wind speed.

are sensibly different between nonlinear and linear models with no foundation damping. On average, the use of the linear model with zero foundation damping results in an overestimate of 19 % of the peak bending moment at the mudline, with a maximum error of about 31 %. Differences are also observed in the DELs, as shown in Fig. 12a. For clarity, the DEL has been normalised by the results obtained from the

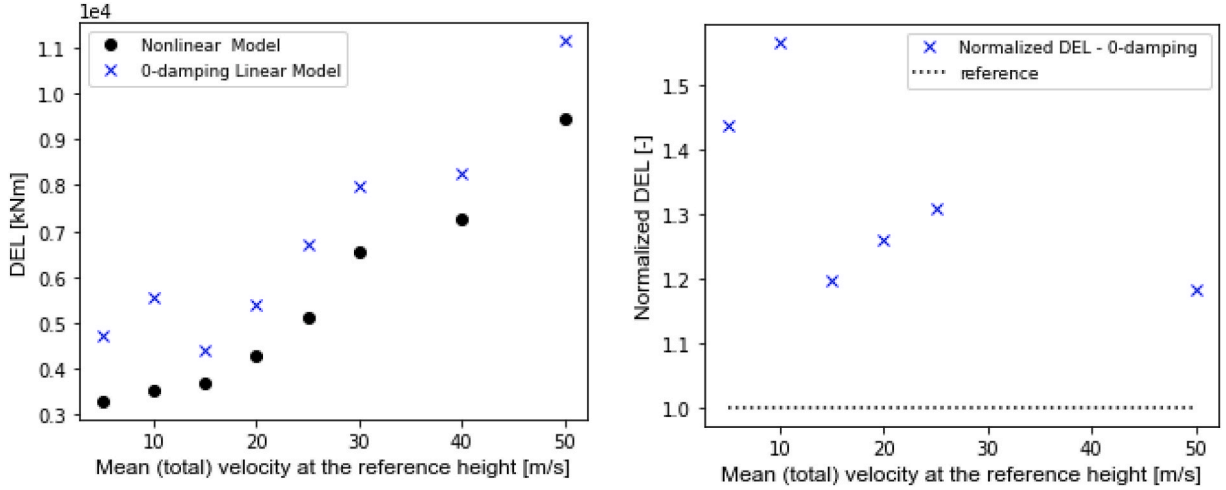

Fig. 12. Damage Equivalent Load for several wind speeds; a) absolute, and b) normalised values.

nonlinear model, in Fig. 12b. On average the linear model with zero damping gives an overestimate of 29 %, and a maximum of about 60 %. These results show the importance of soil-foundation damping in the design of wind tower turbines.

3.2. Optimisation of foundation damping for single wind realisation

In this section, the responses of the linear SSI model to the aerodynamic forces generated at several wind speeds, are presented. A single simulation for each wind speed is considered. For a given wind speed, the same turbulent wind field is used to derive the aerodynamic forcing for both the linear and nonlinear models. Following the method in Section 2.1, the stiffness-proportional coefficient, β, is calibrated to approximate the response of the linear model to the baseline nonlinear results.

3.2.1. Sensitivity analysis

Before performing an optimisation of the stiffness-proportional coefficient, β, a sensitivity analysis is conducted by varying the coefficient between $\beta = 0$ and $\beta = 3$ to obtain information about minimum location and response sensitivity over foundation damping. Fig. 13 shows the outcome of the analysis where the responses are normalised to the baseline nonlinear results. The optimal values can be determined as the one whose normalised response is closest to the unity. In the case of multiple local minima, the optimum can be selected as the one closest to satisfying both criteria, i.e. peak bending moment and DEL. It can be noted in Fig. 13 that not every curve crosses the reference curve. The investigated method does not modify the initial stiffness with an equivalent secant one, hence, there are cases in which the additional artificial damping is insufficient to capture the response exactly. However, for almost all the cases, a minimum value can be found, and the response can be approximated with an error smaller than 10 %. Moreover, both peak mudline bending moment and DEL curves can cross the

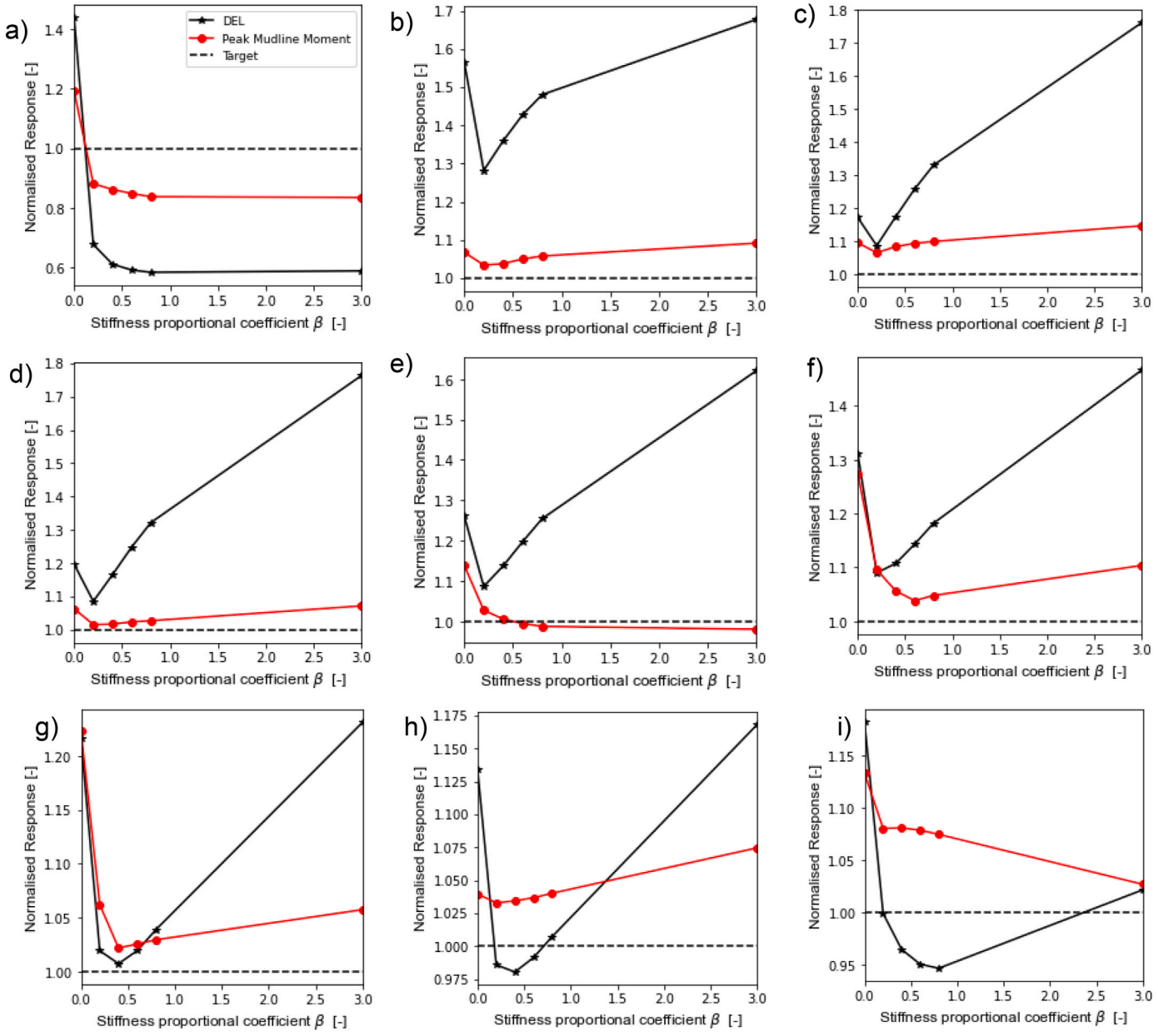

Fig. 13. Sensitivity of the response at the variation of the stiffness proportional damping coefficient β for different wind speeds of a) 5 m/s, b) 10 m/s, c) 12.5 m/s, d) 15 m/s, e) 20 m/s,f) 25 m/s, g) 30 m/s, h) 40 m/s and i) 50 m/s.

reference curve at different wind speeds, but often the local minimum occurs at the same level of damping; therefore, an optimisation procedure can be performed on either objective function, obtaining accurate responses. These results can also be used either as the direct best approximate values or as initial guesses of the numerical optimisation, thereby accelerating convergence.

In Fig. 14, the bending moment time-history functions are shown for a few selected cases; a comparison between the response of the nonlinear baseline model is performed against the linearized model with and without foundation damping. It is evident that the baseline model induces a nonlinear effect on the mudline bending moment; the response does not vary monotonically with the damping level; in some sections of the time series the response is increased for different damping levels, and in other sections, it is reduced. Empirical exceedance probabilities for responses at a wind speed of 10 m/s with six different damping levels are shown in Fig. 15.

For the case $\beta = 1.9$, for higher probabilities, the response is less than the undamped case, but for low probabilities, the response is higher. As the responses do not simply scale with different damping levels, random variability in the results should be also considered. The maximum value observed in any random sequence is subject to large sampling uncertainty. Asymptotically, the width of the confidence interval for the exceedance probability of the largest observation is independent of sample size, when plotted on a log-scale [50]. That is, increasing the simulation length does not decrease the sampling uncertainty associated with the largest observation. Instead, multiple simulations of the same length are required to understand the distribution of the maximum value in a given length of time. Therefore, selecting the optimal damping level based on attempting to match the largest load in the nonlinear simulation is unlikely to return robust results. Instead, some kind of integrated measure of the load, such as a DEL or Kullback–Leibler divergence between response distributions is likely to be more robust to sampling uncertainties. An analysis conducted on multiple realizations is performed in Section 4.

3.2.2. *Optimisation of the maximum bending moment at the mudline*

In this section, numerical optimisation is conducted to minimise the difference between the linear and baseline models regarding the maximum bending moment at the mudline. Initial guesses obtained from the sensitivity analysis are used for the nonlinear optimisation analysis; this is repeated for each wind speed.

Responses of the linear model with optimal stiffness proportional damping coefficient are illustrated in Fig. 16. In Fig. 16a, the absolute maximum bending moments of the baseline model are indicated by black circles while the model with optimal damping is indicated by red crosses. Fig. 16a demonstrates good agreement with the results, which

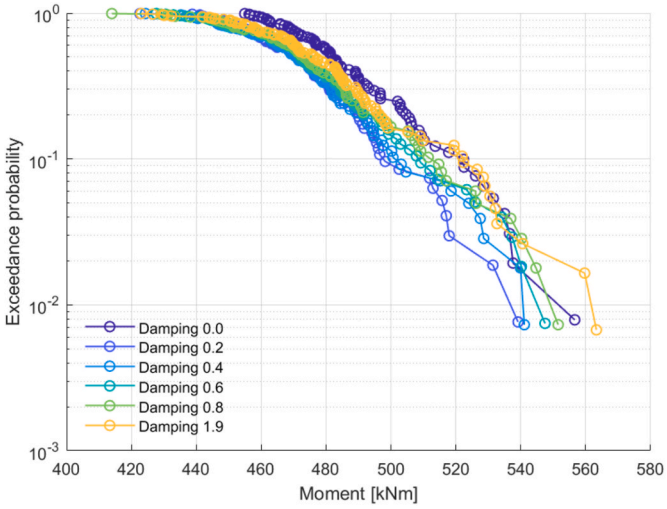

Fig. 15. Empirical exceedance probabilities for mudline bending moments for simulations from the linear model at 10 m/s wind speed, with varying damping levels.

confirms the efficacy of the simplified approach. In addition, the results of the linear model with no foundation damping are indicated in Fig. 16a by blue "X" makers. The average error of 15 % from the undamped model is reduced to 2 % using the optimal stiffness proportional coefficient. For the same analyses, the results for the DEL are presented in Fig. 16b through normalised values. The results of the model with no foundation damping have a mean error of about 29 %, while the results of the model with stiffness proportional damping coefficient have an error of 9 %. It is worth noting that the stiffness proportional damping coefficient was optimized to minimise the error on the bending moment and hence, errors were expected as observed from the sensitivity analysis. On the other hand, as observed from the sensitivity analysis, local minima occur at similar damping levels.

3.2.3. *Optimisation of damping coefficients based on the damage equivalent load*

In this section, numerical optimisation is conducted to minimise the difference in terms of the DEL computed via Eq. (13) for the linear and nonlinear models. The normalised results are shown in Fig. 17a. An excellent match of the response is observed compared to the undamped model, with an average error of about 7 %; moreover, the results are all on the conservative side.

For the same optimized damping values, the peak bending moment values at the mudline are shown in Fig. 17b. Although the optimisation

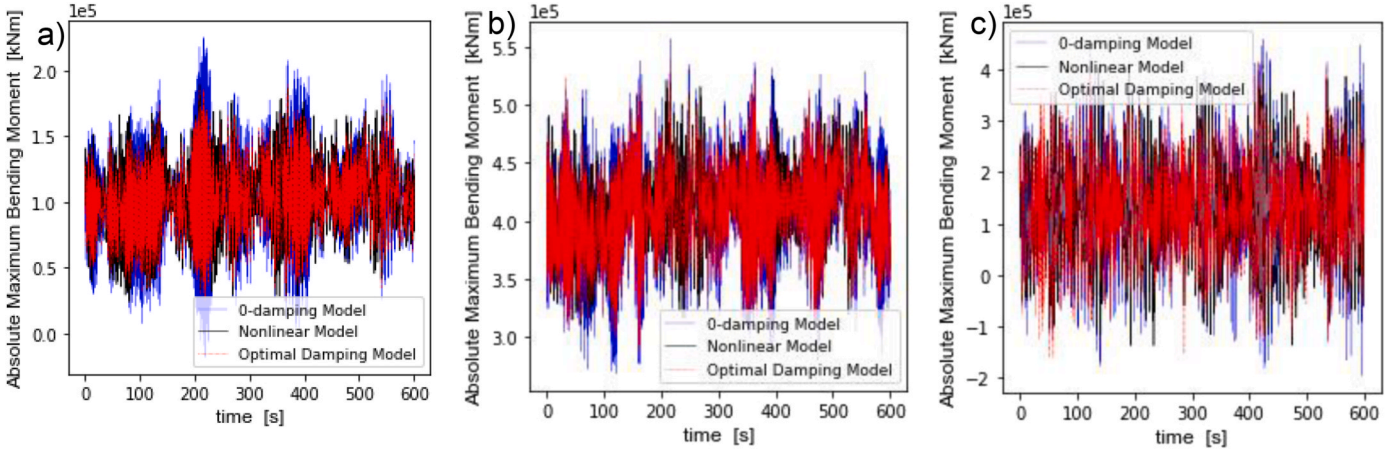

Fig. 14. Time-history bending moment functions at the mudline with and without foundation damping for three wind speeds, a)5 m/s,b) 10 m/s and c) 50 m/s.

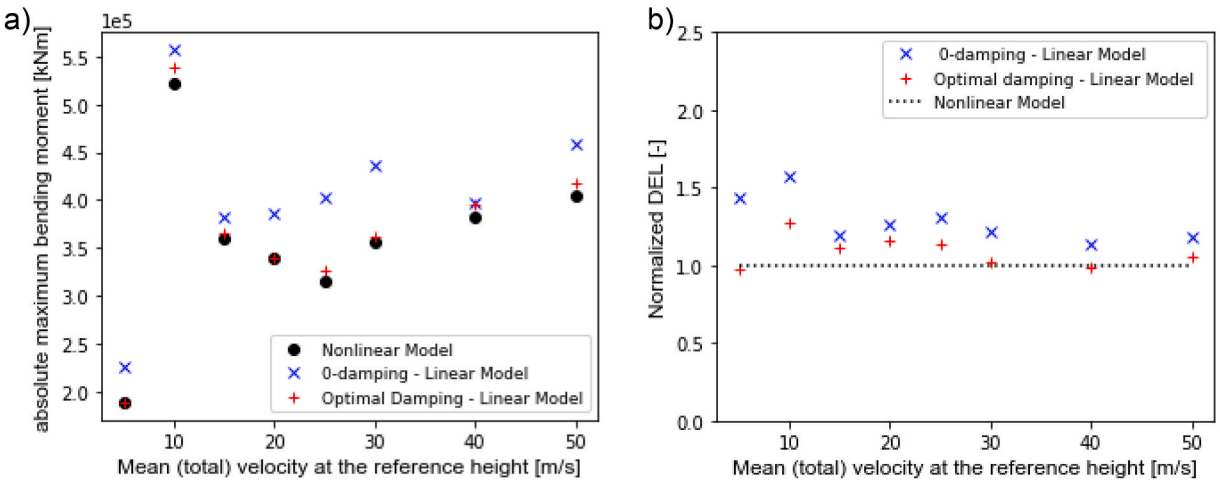

Fig. 16. Responses of the wind turbine models in terms of a) peak bending moment at the mudline, and b) DEL.

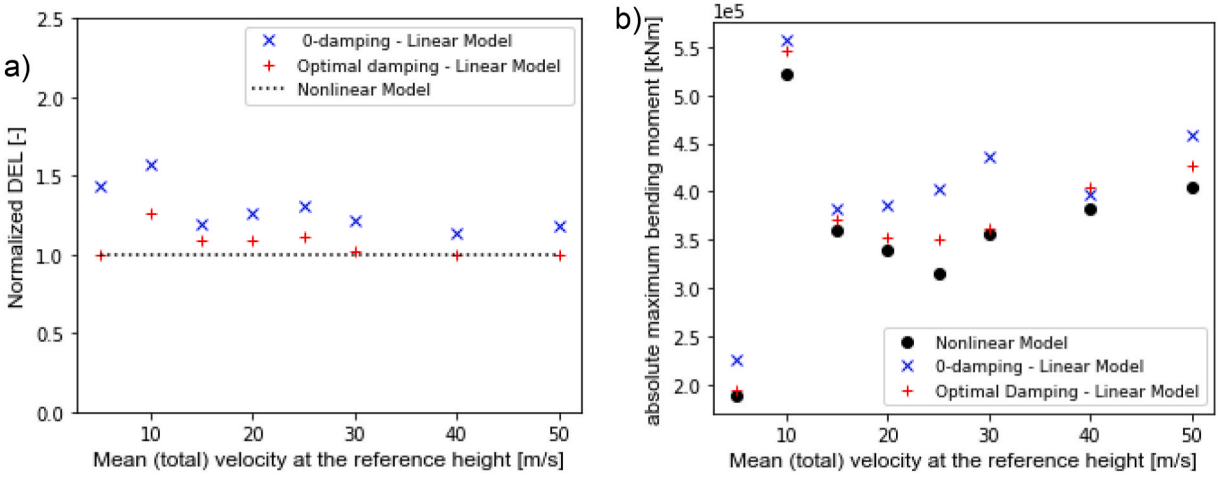

Fig. 17. Responses of the wind turbine models in terms of a) DEL, and b) peak bending moment at the mudline.

has been conducted to minimise the error in the DEL, a better prediction of the peak values is obtained, with an average error that decreases from about 14.1 % for the undamped model to 4.8 % for the model with optimal stiffness-proportional damping.

3.2.4. *Verification through fitted values*

The stiffness-proportional damping coefficients obtained through the two numerical optimisation methods are used to derive empirical relations between the optimal values and the wind speed. In Fig. 18a, the stiffness-proportional damping coefficients obtained by minimizing the

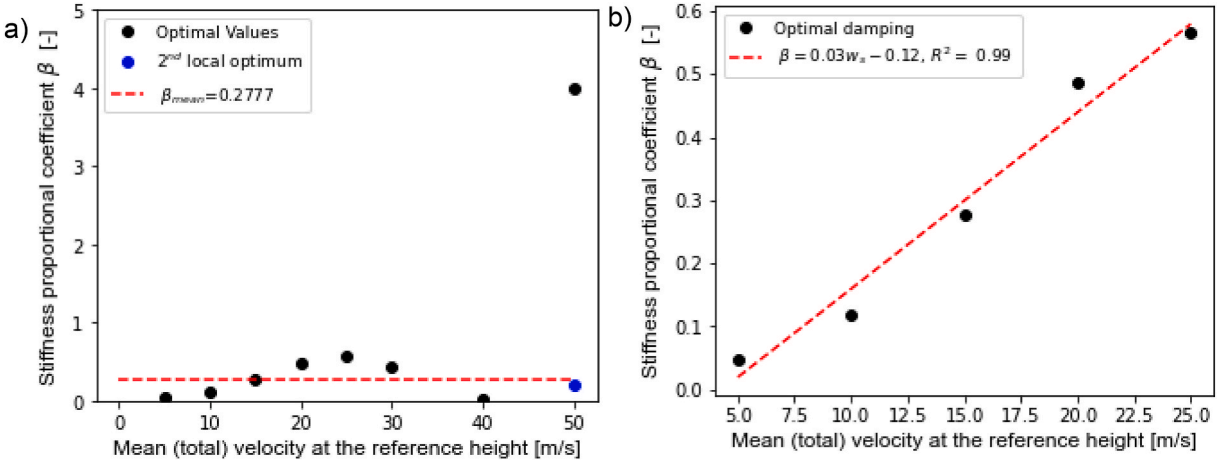

Fig. 18. Optimal stiffness-proportional values to minimise the error on the peak bending moment at the mudline for a) operational and extreme and b) only operational wind speed intervals.

error on the peak bending moment at the mudline are fitted through a constant average value to cover the entire interval of operation and extreme wind. Since two local minima were found in the sensitivity analysis (Fig. 13i), the smaller one has been considered. For operational speeds in the interval of 5 m/s – 25 m/s, a linear regression line is obtained, as depicted in Fig. 18b. Empirical parameters of the fitted curves are indicated in each legend.

Similarly, for the case of optimal values obtained by minimizing the error on DEL, a constant value and linear curve are derived in Fig. 19a and b, respectively. To assess the effectiveness of the fitted values, wind simulations are performed by using the updated foundation damping. Responses of the model with fitted β values are shown in Fig. 20a for the peak bending moment at the mudline and in Fig. 20b for the DEL. A red cross symbol is used for the values optimized for the peak bending moment and a small cyan dot for the optimisation of the DEL. Good results are obtained through both methods, with a mean error of less than 4 % on the peak bending moment and than 6 % on the DEL. The linear best-fit function returns a better accuracy, and a more conservative outcome compared to the constant value approximation.

3.3. Optimisation of foundation damping for random wind realizations

The effect of the random variability in the aerodynamic loads on the optimized damping level is also investigated. Hydrodynamic loading which results in further random variability is not considered in this analysis to focus on the aerodynamic impact on the responses. Ten random turbulent wind fields for each wind speed were generated. Following the method in Section 2.1, the stiffness-proportional viscous damping is calibrated to approximate the average response of the linear model with foundation damping to the mean results of the baseline model.

Fig. 21a shows the maximum bending moments at the mudline for every simulation; their mean and standard deviation values are also reported in Fig. 21b and c, showing the impact of the "static" component or thrust of the aerodynamic forces and the turbulent component, respectively. Variability of the responses is measured through the coefficient of variation (COV) in Fig. 21d. The mean values are similar for most of the cases except a slight dispersion is observed for the wind speed of 10 m/s where high bending moments induce nonlinearities on the soil-pile interaction. However, there is a larger scatter in standard deviation values, with an average coefficient of variation (COV) of about 29 %. This pattern is to be expected since the random turbulent wind fields have the same mean wind speeds, but different random variations about the mean. It is important to note that the damping is predominantly driven by the dynamic effects on the soil-pile system, related to the turbulent wind fields.

3.3.1. Sensitivity analysis

A sensitivity analysis of the dynamic response is performed as in Section 3.2.1 for each realisation of the set of aerodynamic forces, by varying the stiffness-proportional coefficient, between $\beta = 0$ and $\beta = 3$. Fig. 22 shows the outcome of the sensitivity analysis in which the responses are normalised to the baseline nonlinear results for selected wind speeds, i.e. 5 m/s, 15 m/s and 50 m/s. The dashed curves represent the results for each realisation whilst the solid curves represent the mean values. Optimal values of the foundation damping coefficient are different for each realisation and for the same wind speed, the sensitivity curves can or cannot cross the unitary normalised response. For extreme winds, the dispersion increases with the increase of the turbulent component of the aerodynamic forces. The average curves at each wind speed will be used to obtain the optimal values used as the initial guess of the following optimisation procedure.

3.3.2. Optimisation of damping coefficients

To support the findings of the sensitivity study, an optimisation analysis is carried out using two objective functions to minimise the error on the peak bending moment at the mudline and the DEL. Results of the responses for every investigated case are reported in Fig. 23; markers are used to indicate the individual analysis while the dashed lines represent the average of the responses for the four cases, i.e. the baseline model, the linear model with foundation damping optimized to reduce the error on the peak bending moment and the DEL, as well as the response of the linear model without foundation damping. This shows that, after the effects of random variability are removed (by averaging over 10 simulations), the linear model with optimized damping gives results which are close to the average response of the nonlinear model, regardless of which optimisation strategy is used.

The improvement in the accuracy of the response compared to the model without foundation damping is not negligible; moreover, these results evidence the efficacy of considering stiffness-proportional damping in capturing the hysteretic damping of the soil when a low-fidelity model needs to be used.

The computed stiffness-proportional damping values are illustrated in Fig. 24; the dispersion of the optimal values is high (average COV of about 75 %) for the optimisation of the peak bending moment and medium (average COV of about 24 %) for the optimisation of the DEL. Linear regression analysis is carried out on the mean values for each objective function (Fig. 24a and b) shows a good correlation with the distribution of both peak bending moments and DEL values. Additionally, a global mean value, equal to 0.3671 for the peak bending moment

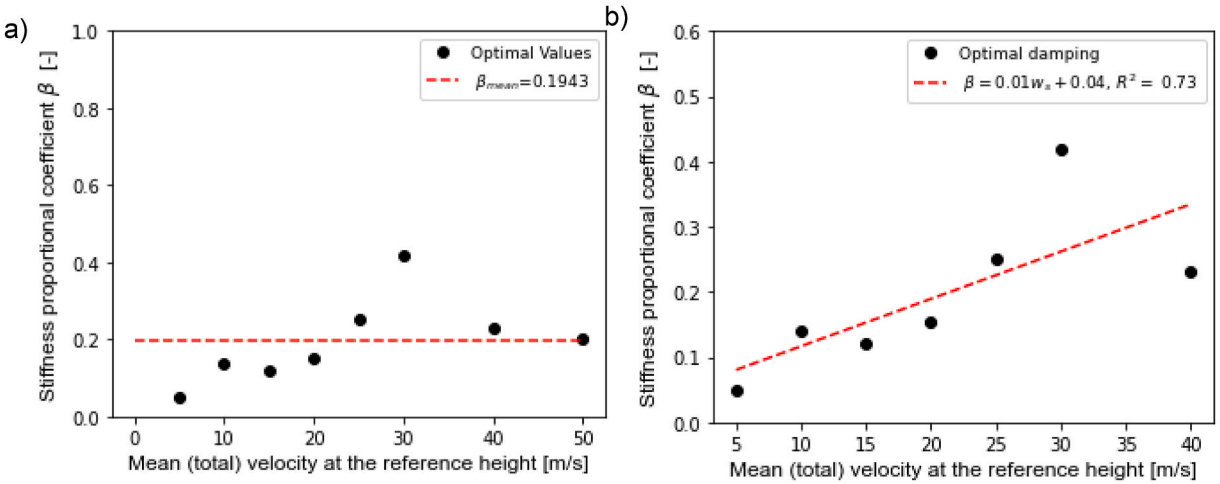

Fig. 19. Optimal stiffness-proportional values to minimise the error of the DEL for a) operational and extreme and b) only operational wind speed intervals.

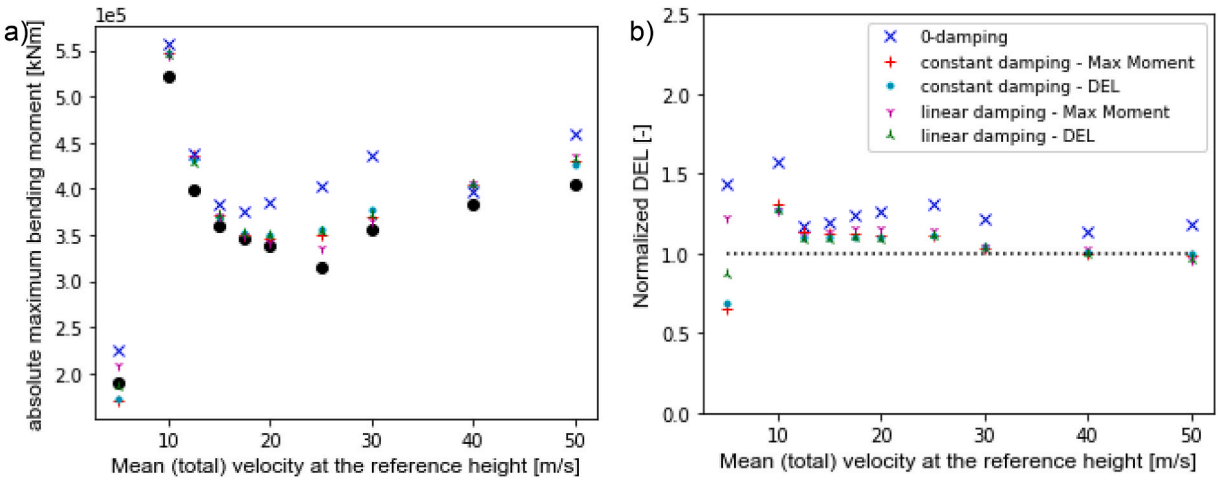

Fig. 20. Verification of the fitted stiffness-proportional damping β in terms of a) peak bending moment at the mudline, and b) DEL.

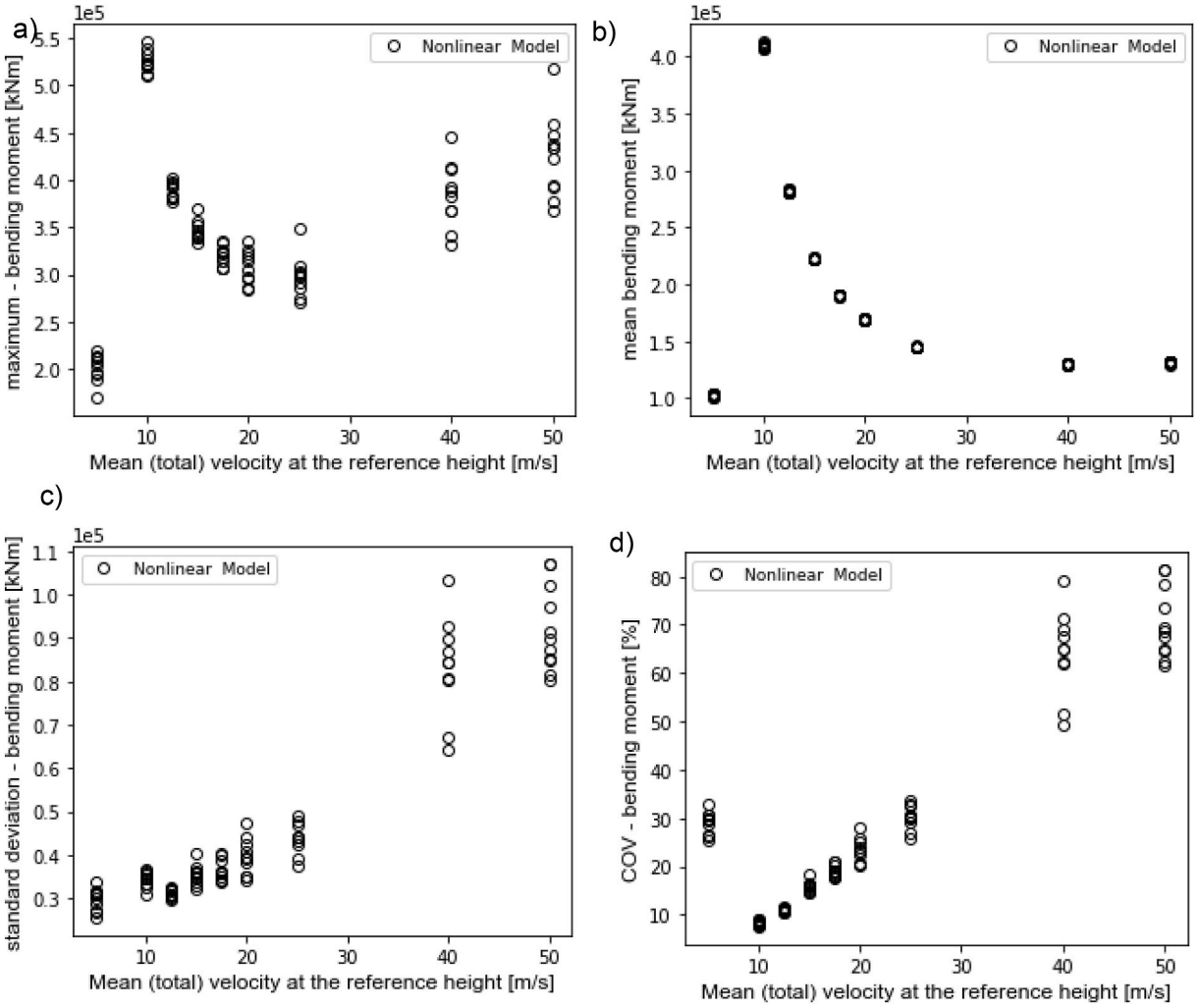

Fig. 21. Distribution of the bending moment time history at the mudline in terms of a)maximum, b) mean, c) standard, and d) coefficient of variation (COV) values.

and 0.1763 for the DEL is also considered for an approximate verification carried out in the next section.

3.3.3. *Verification through averaged values*

The average stiffness-proportional damping values are used to perform a verification of the proposed method, as illustrated in Fig. 25a and b, for the peak bending moment and DEL, respectively. The average responses represented through dashed lines are compared to the baseline responses as well as the responses of the linear model with no foundation damping. Despite an average value being used as foundation

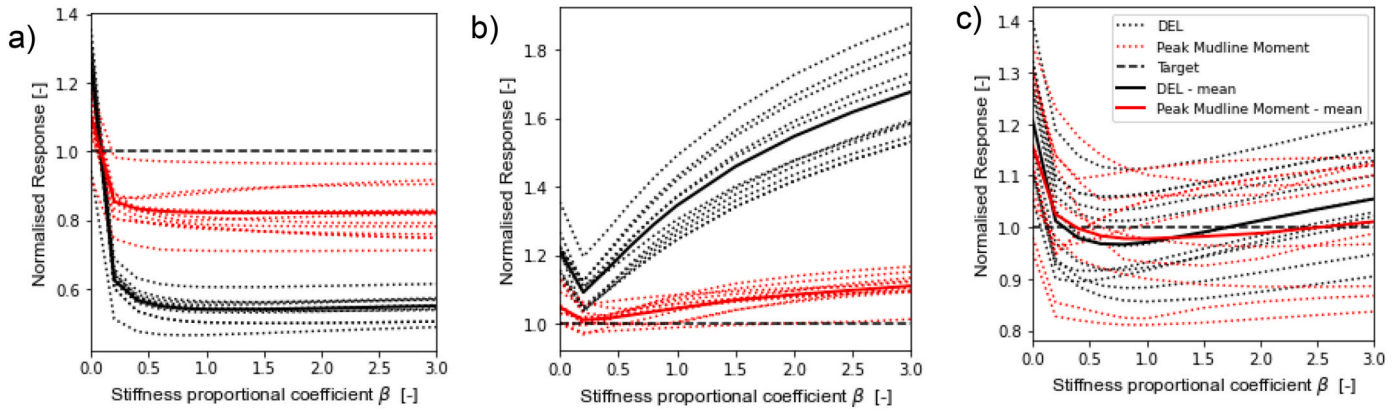

Fig. 22. Sensitivity of the response at the variation of the foundation β for different wind speeds of a) 5 m/s, b) 15 m/s, and c) 50 m/s.

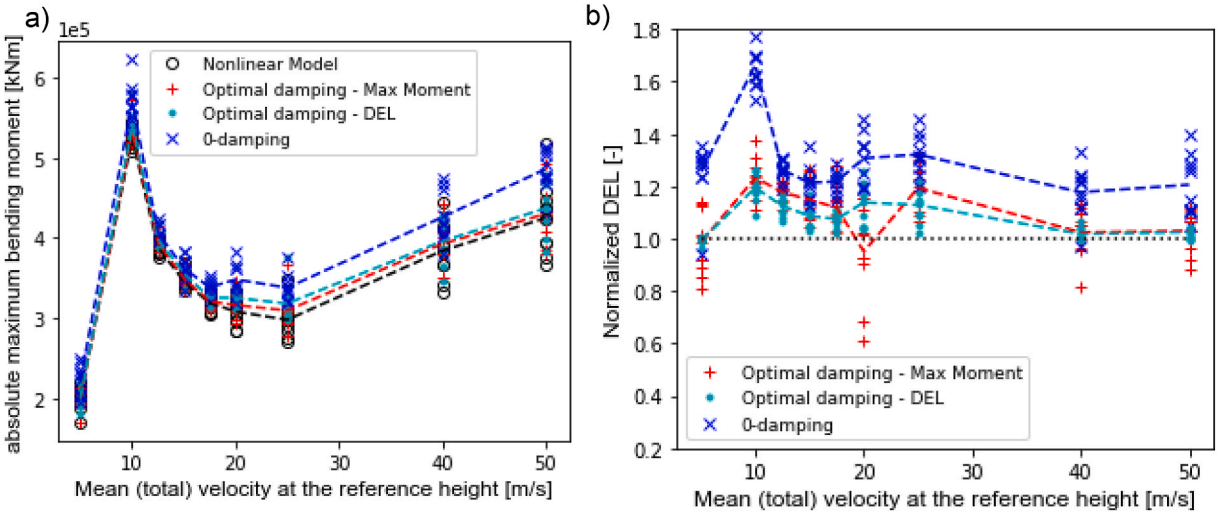

Fig. 23. Responses of the wind turbine models in terms of a) peak bending moment at the mudline, and b) DEL, of the linear model with optimal damping and of the baseline model; dashed lines indicated the average responses.

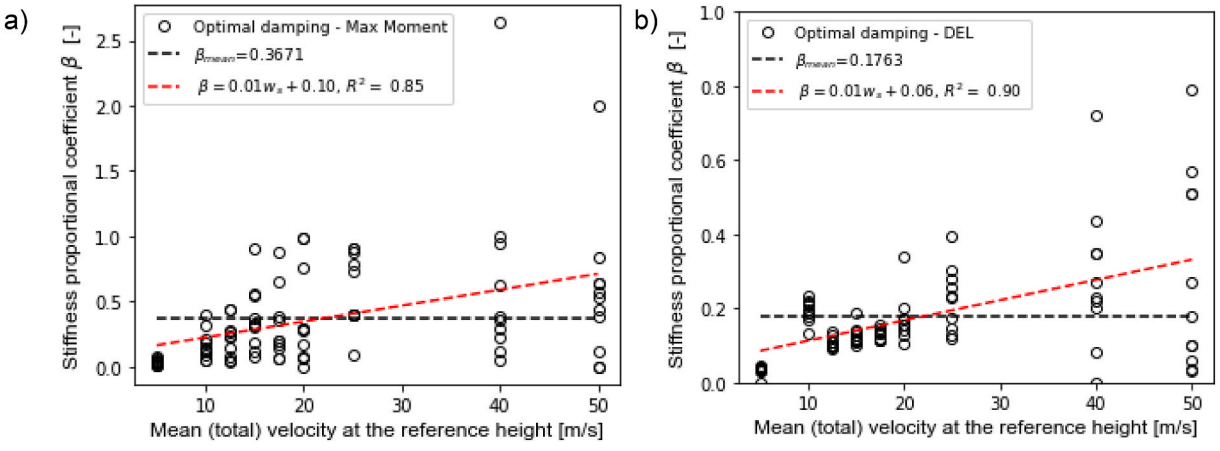

Fig. 24. Regression analysis of the distribution of the mean stiffness-proportional damping values optimized to minimise the error on the a) peak bending moment at the mudline, and b) DEL.

damping, the linearized models capture the effects of the nonlinearities well, reducing the average error compared to the linear model with no foundation damping. Therefore, an improvement in the predictive capability can be obtained by using a simplified approach with stiffness-proportional damping.

The simplified approach generally reduces result dispersion in terms of maximum bending moment and DEL. The average computed COV decreases by approximately 13 %, from 6.8 % with no foundation damping to 5.9 % using the simplified damping approach. Reducing result dispersion mitigates analysis uncertainties and enhances design

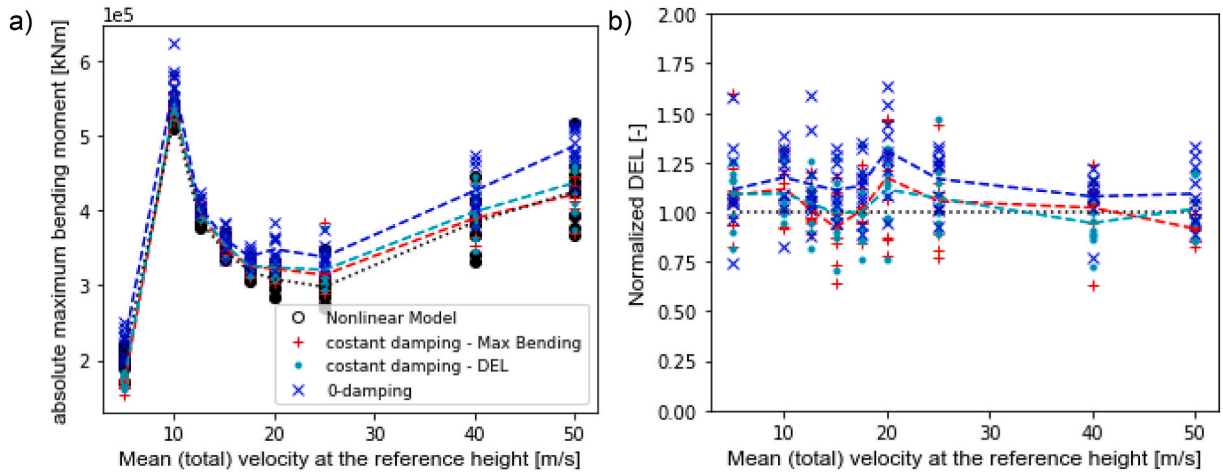

Fig. 25. Verification of the fitted mean stiffness-proportional damping values in terms of a) peak bending moment at the mudline, and b) DEL.

reliability.

4. Limitations of the simplified model

In this study, an investigation on the use of the stiffness proportional damping coefficient to capture soil nonlinearities due to the wind load is conducted. This simplified approach is used to improve the design of the wind towers when low-fidelity models are considered. By retaining the same computational complexity, the stiffness-proportional viscous damping provides a simple and effective approach to enhance the accuracy of the model response, enhancing the quality of the design, and optimizing the wind tower structure and components, avoiding overdesigning.

It is worth emphasizing that the impact of the soil nonlinearities on the dynamic response of the wind tower is twofold; firstly, it increases the overall damping by dissipating energy through material hysteresis in the soil. Secondly, it alters the overall rigidity of the soil-pile-structure system according to the hardening or softening behaviour of the soil. This latter aspect can be relevant since it affects the natural frequencies of the system and hence, its static and dynamic behaviour.

The method investigated in this paper is based on the use of stiffness-proportional damping coefficients, neglecting the modification of the soil-pile stiffness value, which could be done through linear equivalent methods or nonlinear analyses.

Therefore, it should be clarified that the investigated method can be used efficiently when soil-pile deformations are expected to be small, and the modification of the soil stiffness is low. For the case study considered here, the assumption of small soil-pile deformations was reasonable for wind speeds in the range 5 m/s – 50 m/s.

Therefore, a careful consideration of using this approach should be made when.

i. A seismic design should be performed. Converse to the wind loading where the dynamic counterpart is small compared to the static thrust, a ground motion earthquake can produce large dynamic displacements of the pile. In case of low-intensity earthquake events, a substructure method can be applied. Under extreme events, large variations of the soil stiffness cannot be neglected, and a 3D finite element analysis is suggested.
ii. The wind turbine is founded on degrading soils. Whilst wind loads do not produce sensible excess pore pressure built up under operational speeds [51], sandy and clayey soils can suffer fatigue under specific conditions [52] that significantly alters the overall response [45]. In this case, the Allotey and El Naggar's model has implemented a fatigue model [53] that can simulate several cyclic degradation responses.
iii. The soil deposit is a medium-loose sand or soft clay. In this case, the pile should be designed to avoid large deformations. The proposed approach can still be used, although the elastic stiffness of the springs should be computed through a push-over approach to obtain equivalent or secant values.

5. Concluding remarks

Wind turbine design requires thousands of simulations to cover several load cases prescribed by the standards and guidelines. At the preliminary stage, low-fidelity models are used to obtain the first design of the wind turbine tower and components.

Normally, the models used at this stage neglect the nonlinearities induced by the soil-structure interaction effects, since modelling nonlinear SSI requires a large computational demand.

Without altering the complexity of the model, this study investigates the use of a simplified approach through stiffness-proportional viscous damping coefficients applied to the soil-foundation system, to enhance the predictive capability of the low-fidelity models in simulating the dynamic response of wind turbines subjected to wind loading. Low-fidelity models can also be obtained through equivalent linearisation, although this increases the number of evaluations required to obtain equivalent properties and consequently, the computational cost. Alternatively, frequency-dependent models could be a viable solution, although they have not yet been developed for PISA-like models containing rotational springs and are restricted to frequency-domain analysis. The proposed simplified approach is of rapid and easy use for practitioners and represents a viable tool to investigate the impact of the foundation damping on offshore wind turbines.

This paper investigates the relevance of considering soil-foundation damping for the IEA 15 MW reference wind turbine [34], which represents the latest generation of wind turbines and is at an early stage of commercialization. The findings obtained in this case study are listed below.

- In the interval of wind speeds between 5 m/s and 50 m/s, soil nonlinearities are not negligible. The maximum bending moment at the mudline and the DEL obtained through the nonlinear baseline models differ by up to 31 % from the ones computed through the linear model where soil-pile damping is neglected.
- The peak bending moment of the nonlinear model is reduced compared to the linear models, hence, neglecting soil-foundation damping leads to the overdesign of the tower and monopile.
- Similar considerations are observed for the Damage Equivalent Load, with higher values compared to the baseline response, although not occurring for every investigated case.

- The use of stiffness-proportional viscous damping has been proven to be effective in reducing the differences with the baseline model. The simplified method enabled multiple simulations to be run without increasing computational time.
- A regression curve can be used to derive the stiffness-proportional damping coefficients; verification has shown a good improvement in obtaining more accurate results compared to models with no foundation damping, for both deterministic and random analyses.
- The method is efficient and conservative for the computation of the maximum bending moment at the mudline.
- Minimizing the error on the DEL generates less dispersed optimal foundation values on the random analysis. This is because the DEL is an integrated measure of the load, and hence a more robust metric for sampling uncertainties.
- Although the error of the DEL is overall reduced, non-conservative results can be obtained especially at low wind speeds. In that case, nonlinear analyses should be always carried out when fatigue analyses are required to avoid non-conservative outcomes.

In conclusion, this study highlights the importance of accounting for foundation damping in the preliminary design of offshore wind turbines. The simplified approach adopted here, which uses constant stiffness-proportional foundation damping coefficients for both lateral and rotational soil-pile interactions, enhances the accuracy of key dynamic responses, such as the maximum bending moment at the mudline and the DEL. While the results are specific to the case study of the IEA 15 MW reference wind turbine [34], the proposed stiffness-proportional viscous damping approach can be applied to different wind turbines, monopiles, and wind and soil conditions, following the proposed methodology. It is particularly suitable for fast computations when numerous simulations are required.

CRediT authorship contribution statement

Alessandro Tombari: Writing – review & editing, Writing – original draft, Visualization, Supervision, Software, Resources, Project administration, Methodology, Investigation, Funding acquisition, Conceptualization. **Rohollah Rostami:** Writing – original draft, Visualization, Software, Resources, Investigation, Data curation. **Edward Mackay:** Writing – review & editing, Visualization, Investigation, Formal analysis, Conceptualization. **M.H. El Naggar:** Writing – review & editing, Writing – original draft, Supervision, Conceptualization.

Declaration of competing interest

The authors declare the following financial interests/personal relationships which may be considered as potential competing interests: Dr Alessandro Tombari reports financial support was provided by Engineering and Physical Sciences Research Council. If there are other authors, they declare that they have no known competing financial interests or personal relationships that could have appeared to influence the work reported in this paper.

Acknowledgement

Dr Tombari gratefully acknowledges the financial support of the Engineering and Physical Sciences Research Council, UK, through the New Investigator Award EP/W001071/2 “Structural Life-Cycle Enhancement of Next-Generation Onshore and Offshore Wind Farms”.

Data availability

Data are deposited in the University of Exeter Repository (http://hdl.handle.net/10871/140678) and at https://github.com/AntroxEV/ResearchDeposit (DOI: 10.5281/zenodo.15088230)

References

[1] 61400 IEC. *Wind energy generation systems - Part 3-1*: design requirements for fixed offshore wind turbines, International Standard 61400-3–1:2019. Apr. 05, 2019 [Online]. Available: https://webstore.iec.ch/publication/29360.
[2] ISO 19902:2020. Petroleum and natural gas industries — fixed steel offshore structures. ISO 19902; 2020 [Online]. Available: https://www.iso.org/standard/65688.html.
[3] Hübler C, Gebhardt CG, Rolfes R. Development of a comprehensive database of scattering environmental conditions and simulation constraints for offshore wind turbines. Wind Energ. Sci. Oct. 2017;2(2):491–505. https://doi.org/10.5194/wes-2-491-2017.
[4] Hübler C, Gebhardt CG, Rolfes R. Assessment of a standard ULS design procedure for offshore wind turbine sub-structures. J. Phys.: Conf. Ser. Oct. 2018;1104:012013. https://doi.org/10.1088/1742-6596/1104/1/012013.
[5] Damgaard M, Zania V, Andersen LV, Ibsen LB. Effects of soil–structure interaction on real time dynamic response of offshore wind turbines on monopiles. Eng Struct Sep. 2014;75:388–401. https://doi.org/10.1016/j.engstruct.2014.06.006.
[6] Passon P, Kuhn M, Butterfield S, Jonkman J, Camp T, Larsen TJ. OC3 – Benchmark exercise of aero-elastic offshore wind turbine codes: preprint. National Renewable Energy Laboratory; Aug. 2007. Conference Paper NREL/CP-500-41930.
[7] Jasa J, Bortolotti P, Zalkind D, Barter G. Effectively using multifidelity optimization for wind turbine design. Wind Energ. Sci. May 2022;7(3):991–1006. https://doi.org/10.5194/wes-7-991-2022.
[8] Novak M, El Hifnawy L. Structural response to wind with soil-structure interaction. In: Advances in wind engineering. Elsevier; 1988. p. 329–38. https://doi.org/10.1016/B978-0-444-87156-5.50044-8.
[9] Bhattacharya S, Adhikari S. Experimental validation of soil–structure interaction of offshore wind turbines. Soil Dynam Earthq Eng May 2011;31(5–6):805–16. https://doi.org/10.1016/j.soildyn.2011.01.004.
[10] Lombardi D, Bhattacharya S, Muir Wood D. Dynamic soil–structure interaction of monopile supported wind turbines in cohesive soil. Soil Dynam Earthq Eng Jun. 2013;49:165–80. https://doi.org/10.1016/j.soildyn.2013.01.015.
[11] Xu Y, et al. Support condition monitoring of offshore wind turbines using model updating techniques. Struct Health Monit Jul. 2020;19(4):1017–31. https://doi.org/10.1177/1475921719875628.
[12] Shi S, Zhai E, Xu C, Iqbal K, Sun Y, Wang S. Influence of pile-soil interaction on dynamic properties and response of offshore wind turbine with monopile foundation in sand site. Appl Ocean Res Sep. 2022;126:103279. https://doi.org/10.1016/j.apor.2022.103279.
[13] Cheng X, Li M, Ma C, El Naggar MH, Wang P, Sun X. Dynamic analysis of tripod pile foundation in clays for offshore wind turbines. Ocean Eng Nov. 2023;287:115832. https://doi.org/10.1016/j.oceaneng.2023.115832.
[14] Jung S, Kim S-R, Patil A, Hung LC. Effect of monopile foundation modeling on the structural response of a 5-MW offshore wind turbine tower. Ocean Eng Nov. 2015;109:479–88. https://doi.org/10.1016/j.oceaneng.2015.09.033.
[15] Jonkman J, Butterfield S, Musial W, Scott G. Definition of a 5-MW reference wind turbine for offshore system development. NREL, National Renewable Energy Laboratory; Feb. 2009. Technical Report NREL/TP-500-38060.
[16] Damgaard M, Bayat M, Andersen LV, Ibsen LB. Assessment of the dynamic behaviour of saturated soil subjected to cyclic loading from offshore monopile wind turbine foundations. Comput Geotech Sep. 2014;61:116–26. https://doi.org/10.1016/j.compgeo.2014.05.008.
[17] Løken IB, Kaynia AM. Effect of foundation type and modelling on dynamic response and fatigue of offshore wind turbines. Wind Energy Dec. 2019;22(12):1667–83. https://doi.org/10.1002/we.2394.
[18] Simpson T, Dervilis N, Couturier P, Maljaars N, Chatzi E. Reduced order modeling of non-linear monopile dynamics via an AE-LSTM scheme. Front Energy Res Mar. 2023;11:1128201. https://doi.org/10.3389/fenrg.2023.1128201.
[19] Matlock H. Correlation for design of laterally loaded piles in soft clay. In: The offshore technology conference; Apr. 1970. https://doi.org/10.4043/1204-MS.
[20] Reese L, Cox W, Koop F. Field testing and analysis of laterally loaded piles on stiff clay. In: The offshore technology conference; May 1975. https://doi.org/10.4043/2312-MS.
[21] El Naggar MH, Novak M. Nonlinear analysis for dynamic lateral pile response. Soil Dynam Earthq Eng Jun. 1996;15(4):233–44. https://doi.org/10.1016/0267-7261(95)00049-6.
[22] Jeanjean P, Zakeri A, Zhang Y, Andersen KH. The New ISO/API P-Y curves in clays and their reconciliation with the PISA framework. In: Day 1 Mon, may 02, 2022. Houston, Texas, USA: OTC; Apr. 2022. https://doi.org/10.4043/31860-MS. D011S014R004.
[23] Brandenberg SJ, Zhao M, Boulanger RW, Wilson DW. p-y plasticity model for nonlinear dynamic analysis of piles in liquefiable soil. J Geotech Geoenviron Eng Aug. 2013;139(8):1262–74. https://doi.org/10.1061/(ASCE)GT.1943-5606.0000847.
[24] Heidari M, El Naggar H, Jahanandish M, Ghahramani A. Generalized cyclic p–y curve modeling for analysis of laterally loaded piles. Soil Dynam Earthq Eng Aug. 2014;63:138–49. https://doi.org/10.1016/j.soildyn.2014.04.001.
[25] Heidari M, Hesham El Naggar M. Analytical approach for seismic performance of extended pile-shafts. J Bridge Eng Oct. 2018;23(10):04018069. https://doi.org/10.1061/(ASCE)BE.1943-5592.0001272.

[26] Bisoi S, Haldar S. Dynamic analysis of offshore wind turbine in clay considering soil–monopile–tower interaction. Soil Dynam Earthq Eng Aug. 2014;63:19–35. https://doi.org/10.1016/j.soildyn.2014.03.006.
[27] Corciulo S, Zanoli O, Pisanò F. Transient response of offshore wind turbines on monopiles in sand: role of cyclic hydro–mechanical soil behaviour. Comput Geotech Mar. 2017;83:221–38. https://doi.org/10.1016/j.compgeo.2016.11.010.
[28] Sun Y, Xu C, Du X, El Naggar MH, Zhang X, Jia J. Nonlinear lateral response of offshore large-diameter monopile in sand. Ocean Eng Nov. 2020;216:108013. https://doi.org/10.1016/j.oceaneng.2020.108013.
[29] Sunday K, Brennan F. Influence of soil–structure modelling techniques on offshore wind turbine monopile structural response. Wind Energy Jun. 2022;25(6):998–1012. https://doi.org/10.1002/we.2711.
[30] Versteijlen WG, Metrikine AV, Van Dalen KN. A method for identification of an effective Winkler foundation for large-diameter offshore wind turbine support structures based on in-situ measured small-strain soil response and 3D modelling. Eng Struct Oct. 2016;124:221–36. https://doi.org/10.1016/j.engstruct.2016.06.007.
[31] Malekjafarian A, Jalilvand S, Doherty P, Igoe D. Foundation damping for monopile supported offshore wind turbines: a review. Mar Struct May 2021;77:102937. https://doi.org/10.1016/j.marstruc.2021.102937.
[32] Versteijlen WG, Renting FW, Van Der Valk PLC, Bongers J, Van Dalen KN, Metrikine AV. Effective soil-stiffness validation: shaker excitation of an in-situ monopile foundation. Soil Dynam Earthq Eng Nov. 2017;102:241–62. https://doi.org/10.1016/j.soildyn.2017.08.003.
[33] Carswell W, et al. Foundation damping and the dynamics of offshore wind turbine monopiles. Renew Energy Aug. 2015;80:724–36. https://doi.org/10.1016/j.renene.2015.02.058.
[34] Gaertner E, et al. Definition of the IEA 15-megawatt offshore reference wind turbine'. International Energy Agency; 2020 [Online]. Available: https://www.nrel.gov/docs/fy20osti/75698.pdf.
[35] Bardet JP, Ichii K, Lin CH. Eera - a computer program for equivalent-linear earthquake site response analyses of layered soil deposits. University of Southern California; 2000.
[36] Kausel E, Assimaki D. Seismic simulation of inelastic soils via frequency-dependent moduli and damping. J Eng Mech Jan. 2002;128(1):34–47. https://doi.org/10.1061/(ASCE)0733-9399(2002)128:1(34).
[37] Toft HS, Sørensen JD. Reliability-based design of wind turbine blades. Struct Saf Sep. 2011;33(6):333–42. https://doi.org/10.1016/j.strusafe.2011.05.003.
[38] Yu C, Lv X, Huang D, Jiang D. Reliability-based design optimization of offshore wind turbine support structures using RBF surrogate model. Front Struct Civ Eng Jul. 2023;17(7):1086–99. https://doi.org/10.1007/s11709-023-0976-8.
[39] Padrón LA, Carbonari S, Dezi F, Morici M, Bordón JDR, Leoni G. Seismic response of large offshore wind turbines on monopile foundations including dynamic soil–structure interaction. Ocean Eng Aug. 2022;257:111653. https://doi.org/10.1016/j.oceaneng.2022.111653.
[40] Seismosoft. *SeismoStruct v6*.0 - verification report. 2023 [Online]. Available: www.seismosoft.com.
[41] Burd HJ, et al. PISA design model for monopiles for offshore wind turbines: application to a marine sand. Geotechnique Nov. 2020;70(11):1048–66. https://doi.org/10.1680/jgeot.18.P.277.
[42] Jonkman J. The New modularization framework for the FAST wind turbine CAE tool. In: *51st AIAA aerospace Sciences Meeting including the New horizons Forum and aerospace exposition*, grapevine (Dallas/Ft. Worth region). Texas: American Institute of Aeronautics and Astronautics; Jan. 2013. https://doi.org/10.2514/6.2013-202.
[43] Jonkman BJ. TurbSim user's guide: version 1.50. National Renewable Energy Laboratory; Sep. 2009. Technical Report NREL/TP-500-46198.
[44] Allotey N, El Naggar MH. Generalized dynamic Winkler model for nonlinear soil–structure interaction analysis. Can Geotech J Apr. 2008;45(4):560–73. https://doi.org/10.1139/T07-106.
[45] Tombari A, El Naggar MH, Dezi F. Impact of ground motion duration and soil non-linearity on the seismic performance of single piles. Soil Dynam Earthq Eng Sep. 2017;100:72–87. https://doi.org/10.1016/j.soildyn.2017.05.022.
[46] Smith M. ABAQUS/Standard user's manual. United States: Dassault Systèmes Simulia Corp; 2023.
[47] API. Recommended practice for planning, designing and constructing fixed offshore platforms. Washington, D.C: American Petroleum Institute (API); 2007.
[48] Fan K, Gazetas G, Kaynia A, Kausel E, Ahmad S. Kinematic seismic response of single piles and pile groups. J. Geotech. Engrg. Dec. 1991;117(12):1860–79. https://doi.org/10.1061/(ASCE)0733-9410(1991)117:12(1860).
[49] Velarde J, Kramhøft C, Sørensen JD, Zorzi G. Fatigue reliability of large monopiles for offshore wind turbines. Int J Fatig May 2020;134:105487. https://doi.org/10.1016/j.ijfatigue.2020.105487.
[50] Mackay E, Jonathan P. Sampling properties and empirical estimates of extreme events. Ocean Eng Nov. 2021;239:109791. https://doi.org/10.1016/j.oceaneng.2021.109791.
[51] Stuyts B, Weijtjens W, Gkougkoudi-Papaioannou M, Devriendt C, Troch P, Kheffache A. Insights from in-situ pore pressure monitoring around a wind turbine monopile. Ocean Eng Feb. 2023;269:113556. https://doi.org/10.1016/j.oceaneng.2022.113556.
[52] Allotey N, El Naggar MH. A consistent soil fatigue framework based on the number of equivalent cycles. Geotech Geol Eng 2008;26(1):65–77. https://doi.org/10.1007/s10706-007-9147-2.
[53] Allotey N, El Naggar MH. A numerical study into lateral cyclic nonlinear soil–pile response. Can Geotech J Sep. 2008;45(9):1268–81. https://doi.org/10.1139/T08-050.